OXFORD

Cerebral Cortex, March 2020;30: 1068–1086

doi: 10.1093/cercor/bhz149
Advance Access Publication Date: 13 August 2019
Original Article

ORIGINAL ARTICLE

Pulvinar Modulates Contrast Responses in the Visual Cortex as a Function of Cortical Hierarchy

Bruno Oliveira Ferreira de Souza†, Nelson Cortes† and Christian Casanova

School of Optometry, Université de Montréal, Quebec, CP 6128 Canada

Address correspondence to Christian Casanova, School of Optometry, Université de Montréal, Succ Centre-Ville Montréal, Québec, CP 6128, Canada H3C-3J7. Email: christian.casanova@umontreal.ca.

†These authors equally contributed to this manuscript

Abstract

The pulvinar is the largest extrageniculate visual nucleus in mammals. Given its extensive reciprocal connectivity with the visual cortex, it allows the cortico-thalamocortical transfer of visual information. Nonetheless, knowledge of the nature of the pulvinar inputs to the cortex remains elusive. We investigated the impact of silencing the pulvinar on the contrast response function of neurons in 2 distinct hierarchical cortical areas in the cat (areas 17 and 21a). Pulvinar inactivation altered the response gain in both areas, but with larger changes observed in area 21a. A theoretical model was proposed, simulating the pulvinar contribution to cortical contrast responses by modifying the excitation-inhibition balanced state of neurons across the cortical hierarchy. Our experimental and theoretical data showed that the pulvinar exerts a greater modulatory influence on neuronal activity in area 21a than in the primary visual cortex, indicating that the pulvinar impact on cortical visual neurons varies along the cortical hierarchy.

Key words: cat, lateral posterior nucleus, reversible inactivation, transthalamic pathway, ventral stream

Introduction

The perception of external stimuli is traditionally considered to result solely from the processing of thalamic signals through direct cortico-cortical connections between areas organized in a hierarchical manner (Panagiotaropoulos et al. 2014). This corticocentric view has been challenged in recent years since, besides direct communication between cortical areas through cortico-cortical connections, indirect communication through corticothalamocortical projections can also occur (Casanova 2004; Sherman and Guillery 2013). In the visual system, the pulvinar, which is the largest extrageniculate nucleus in mammals, is a key structure for the transfer of information between cortical areas (Casanova 2004; Chalfin et al. 2007). It receives the main input from the primary visual cortex and from most if not all higher-order visual areas and, in turn, projects back to these areas (Supplementary Fig. S1; Leh et al. 2008; Arcaro et al. 2015; Barron et al. 2015). Pulvinar neurons have cortex-like receptive fields and this structure has been associated with a number of normal vision processing such as higher-order motion, feature binding, and attention (Petersen et al. 1987; Chalupa and Abramson 1989; Casanova and Savard 1996; Merabet et al. 1998; Ward et al. 2002). It has recently been suggested that deficits in sensory processing observed in disorders such as schizophrenia results from a dysfunction in transthalamic cortical communication involving the pulvinar (Byne et al. 2009; Benarroch 2015).

Although much is known about the geniculo-cortical pathway, we have virtually no information about the functional properties of the much more extensive pulvinar-cortical circuits. Consequently, their contribution in cortical processing, and ultimately in perception, remains elusive. Attempts to define

the function of these pathways are mainly based on anatomical grounds (Sherman and Guillery 2013). Two types of inputs, drivers and modulators, have been described along the well-characterized retinogeniculate-cortical pathway on the basis of electrophysiological and anatomical criteria (Sherman and Guillery 1998). In essence, drivers determine the properties of their target cells whereas modulators provide contextual activity modulation of the recipient neurons, and it has been proposed that a general rule, thalamic terminals ending in layer I and IV are modulatory and drivers, respectively (Crick and Koch 1998; Jones 2001; Lee and Sherman 2008; Viaene et al. 2011). In addition, drivers and modulators would yield correspondingly additive/subtractive and multiplicative/divisive changes on the membrane potential of a cortical neuron (Anderson et al. 2000; Chance et al. 2002; Abbott and Chance 2005).

The main cortical inputs to the pulvinar come from layers V neurons in the primary visual cortex and from layers VI neurons in higher-order areas (Lund et al. 1975; Trojanowski and Jacobson 1977; Raczkowski and Rosenquist 1983; Abramson and Chalupa 1985). Anatomical and physiological data indicate that the signals from area 17 are almost exclusively drivers while those from higher-order areas are drivers and modulators (Theyel et al. 2010), with an increase of the modulators/driver ratio along the cortical hierarchy (Huppé-Gourgues et al. 2006). Pulvinar projections to the visual cortex are 2-fold: For the most part, they reach layer I of the primary visual cortex and end in layer IV of all other visual areas (Benevento and Rezak 1976; Ogren and Hendrickson 1977; Rezak and Benevento 1979; Symonds et al. 1981; Roth et al. 2016). Based on this organization, one would suggest that the pulvinar modulates entrant activity in the primary visual cortex and drive neurons in higher-order areas. Thus, the aim of the present study was to test this assumption by investigating the impact of pulvinar on the contrast response function (CRF) of two hierarchically distinct areas in the cat, the primary visual cortex and area 21a (the homolog of V4 in primates, (Payne 1993)). In cats, the pulvinar consists of a group of three nuclei named the lateral posterior-pulvinar complex (LP-pulvinar, (Hutchins and Updyke 1989)). The lateral part of the LP (LPl) is the striato-recipient zone of the LP while the medial part (LPm) is the tectorecipient zone (Abramson and Chalupa 1985; Casanova et al. 1997). LPl neurons project to layer I of area 17 while those in LPl and LPm project to layer IV of area 21a (Miller et al. 1980; Symonds et al. 1981; Berson and Graybiel 1983). Therefore, according to the framework described above, we hypothesize that the CRF of cortical neurons will be distinctly affected in the two cortical areas: Pulvinar should principally modulate activity (response gain; slope control) in area 17, while it should mainly drive neuronal discharges (contrast gain; baseline control) in area 21a (Fig. 1).

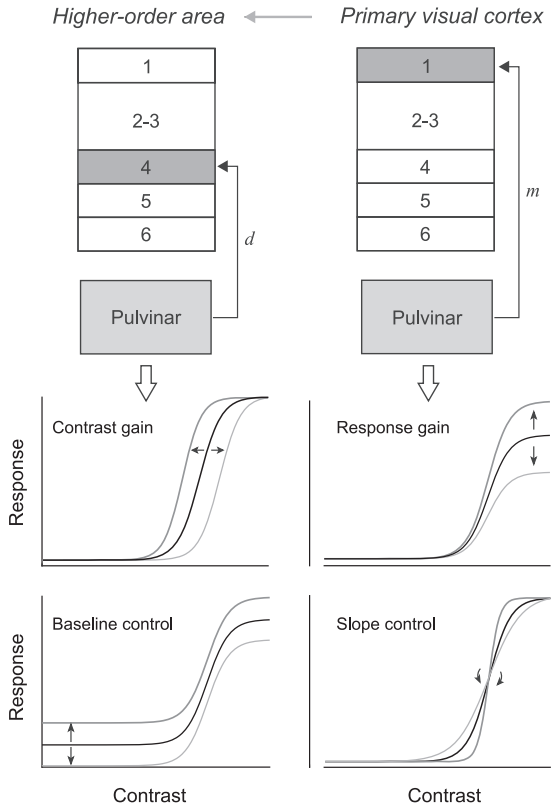

Figure 1. Hypothetical scheme of the nature of pulvino-cortical inputs to the primary visual cortex and an extrastriate area. A putative modulator (m) input would yield non-linear effects on the CRF of neurons from the primary visual cortex represented as changes in the response gain and slope. On the other hand, a putative driver (d) input in higher-order cortical areas would yield linear effects on the neurons' CRFs, characterized by changes in the contrast gain and baseline.

Materials and Methods

Animals and Surgery

Experiments were performed on normal male and female adult cats (2.5–3.5 kg). A total number of 6 animals were used in the present study. All surgical and experimental procedures were undertaken according to the guidelines of the Canadian Council on Animal Care and were approved by the Ethics Committee of the University of Montreal (CDEA 19-008). First, atropine (0.1 mg/kg) and acepromazine (Atravet, 1 mg/kg) were administered subcutaneously to reduce parasympathetic effects of anesthesia and to provoke sedation, respectively. Anesthesia induction was performed with 3.5% Isoflurane in a 50:50 (v/v) gas mixture of O_2 and N_2O. Isoflurane concentration was maintained at 1.5% throughout surgical procedures. A tracheotomy was performed, and animals were immobilized using an intravenous bolus injection of 2% gallamine triethiodide. Then, animals were artificially ventilated and a 1:1 (v/v) solution of 2% gallamine triethiodide (10 mg/kg/h) in 5% of dextrose in lactated ringer was continuously administered intravenously to maintain muscular relaxation and to provide nutrition and electrolytes. Expired level of CO_2 was maintained between 35 and 40 mmHg by adjusting the tidal volume and respiratory rate. Heart rate was continuously monitored during the experiment and the temperature was maintained at 37 °C by means of a feedback controlled heated blanket. Local anesthetic (lidocaine hydrochloride 2%) was used in all incisions and pressure points. Dexamethasone (4 mg, I.M.) was administered every 12 h in order to avoid cortical swelling. Pupils were dilated using atropine (Mydriacyl) and nictitating membranes were retracted using phenylephrine (Midfrin). Rigid contact lenses with the appropriate power were used to correct eyes refraction and eye lubricants were used to avoid corneal dehydration. Three craniotomies were performed in order to gain access to the LP nucleus (5-8A; 3–7 L, Horsley–Clarke coordinates) and to cortical areas 17 (4-8P; 0.5–2 L) and 21a (2-6P; 7–11 L). Small durectomies were performed for each electrode penetration. A

2% Agar solution in saline was applied over the exposed regions to increase recordings stability and to avoid the drying of the cortical surface.

Visual Stimuli

Visual stimuli were generated using the VPixx software (VPixx Technologies Inc., St-Bruno, QC, Canada), projected onto an isoluminant screen located at 57 cm of viewing distance and covering 116° by 150° of visual angle with a mean luminance of 25 cd/m^2. Stimuli consisted of drifting sinusoidal gratings with spatial and temporal frequencies set at 0.3 cpd and 3 Hz for all stimuli, respectively. The spatial and temporal frequencies were inside the response range of neurons from both areas 17 (Movshon et al. 1978; Zhang et al. 2017) and 21a (Tardif et al. 1996; Morley and Vickery 1997; Villeneuve et al. 2009). Neurons' direction tuning was obtained with 50% contrast gratings moving over 360° at 12 steps of 30°. The CRF was evaluated by varying contrast values between 6% and 100% at the neuron's optimal direction. For all tests, trials were fully randomized and each stimulus was presented for at least 10 times. Stimulus presentation lasted 1 and 2 s for contrast and direction tests, respectively, separated by a mean luminance gray screen (blank) used to assess spontaneous activity.

Electrophysiological Recordings and Signal Preprocessing

During recording sessions, the anesthesia was changed to Halothane (0.5–0.8%). This was done to maintain the cortical responsiveness since it has been shown that isoflurane yields a strong depression of visual responses (Villeneuve and Casanova 2003). Neural activity in areas 17 and 21a was recorded using 32-channel linear probes (~1 MΩ, 1×32-6 mm-100-177, Neuronexus). Prior to insertion, the probes were covered with a fluorescent dye (DiI) allowing the histologic assessment of the electrode position in the cortex. Electrophysiological signals were acquired at 30 KHz and band pass filtered between 1 and 7500 Hz using an open-source system (Open-Ephys platform, (Siegle et al. 2017)). Single units were identified using the software package Klusta (Rossant et al. 2016). In brief, signals were high-pass filtered at 500 Hz and a threshold was used to detect the spikes. Subsequently, the spikes were separated by an unsupervised automatic clustering algorithm using principal component analysis. Finally, a manual validation of the clustering process was undertaken. Units exhibiting low spike amplitudes or ill-defined cluster margins were excluded. Peristimulus time histograms (PSTHs) were obtained from the neuronal responses to drifting gratings and the responses of each unit were calculated as the average firing rate during the stimulus presentation for each trial. Units with low firing rates (maximal discharge was <5 spikes/s) in the control condition were excluded from the analysis.

Thalamic Inactivation

The LPl and LPm subdivisions of the LP nucleus were pharmacologically inactivated by the intracerebral injection of a solution of 20 mM gamma aminobutyric acid (GABA) stained with Chicago Sky Blue (0.5%) for the histologic assessment of the location and extent of the injection (Supplementary Fig. S2). The GABA solution was injected using a custom-made injectrode (Lai et al. 2015). First, the solution was injected at a rate of 80 nL/min until the inhibition of the neuronal activity was achieved. A successful inactivation was characterized by the silencing of the local multiunit activity recorded through the injectrode. Subsequently, the injection rate was reduced to 20–40 nL/min to silence neural activity throughout the testing period. The approximate total volume of GABA solution injected was 1 µL. The local neuronal activity was continuously monitored and a recovery from inhibition was observed about 30–45 min after the completion of the GABA injection. Cortical responses were recorded before (control), during (injection), and after (recovery) GABA injection in the thalamus (Supplementary Fig. S2).

Curve Fitting and Data Analysis

The CRF was generated by fitting the Naka–Rushton equation to experimental data:

$$R(C) = R_{\max}\frac{C^n}{C^n + C50^n} + \mathrm{Bsln}, \quad (1)$$

where $R(C)$ is the output response at contrast C, Bsln is the baseline response, n represents the slope of the curve, $R_{\max}$ is the maximum response above the baseline, and C50 is the contrast that evokes half of $R_{\max}$.

The goodness of fit was assessed by a modified version of the chi-squared (χ^2) test that takes into account the linear correlation between the cortical neuronal activity and the response variance. The χ^2 term was considered as:

$$\chi^2 = \sum_i \frac{(e_i - o_i)^2}{k + o_i\frac{\rho_i}{t}}, \quad (2)$$

where i represents the index of the contrast level, o is the observed neuronal response, e is the expected response from the fit, ρ corresponds to the ratio between the response variance and the average firing rate at a particular contrast, t represents the response duration in seconds and k is a small factor ($k = 0.01(P^*\max(o))$) used to avoid infinite values at zero response (Cavanaugh et al. 2002). Due to the nature of our experimental protocol (long-lasting recordings), several factors could affect the recording reliability over time. Consequently, we excluded from the analysis neurons that showed χ^2 values higher than twice the one from the control curve.

The parameters extracted from the curve fit were used to compare the cortical activity recorded during the control, injection, and recovery periods. The $R_{\max}$ and baseline (Bsln) were normalized to the average firing rate at maximum contrast in the control condition. In addition, the percentage of variation (*% Var*) for each CRF parameter (*Par*) was calculated as

$$\%Var = 100 \times \frac{Par_{\mathrm{control}} - Par_{\mathrm{injection}}}{Par_{\mathrm{control}} + Par_{\mathrm{injection}}} \quad (4)$$

The response modulation to drifting gratings was assessed to identify simple and complex-like cells. Fourier transformation of the PSTH was performed and a modulation index was obtained by calculating the ratio of the amplitude of the first harmonic over the DC amplitude (F1/F0). Cells with F1/F0 values greater than one were classified as simple while those with values below one were considered as complex (Skottun et al. 1991).

Selection of CRF Based on the Percentage of Overlap Between Conditions

For each unit, a qualitative analysis of the CRFs obtained in control, injection and recovery conditions were performed by considering the degree of overlap between the confidence intervals (CIs) of each curve. The CIs were estimated by a bootstrapping method. For each contrast curve, a distribution of CRFs was generated by applying the curve fit (equation 1) to resampled datasets over 1000 iterations. The central 95% of the curves' distribution was considered as the CI. Subsequently, the percentages of overlapped areas between the CRFs CIs at control and injection (Ctr-Inj), control and recovery (Ctr-Rec), and injection and recovery (Inj-Rec) were calculated. A 100% overlap between CRF areas indicates that they are equal, while 0% shows that the CRFs are completely different. Neurons exhibiting lower Inj-Rec overlap (Inj-Rec < 50%) and higher Ctr-Rec overlap (Ctr-Rec > 50%) recovered completely from the GABA injection. On the other hand, those with high Inj-Rec overlap were considered partially recovered. However, neurons were only considered partially recovered when their recovery CRFs tended toward the control condition, otherwise they were eliminated from the analysis.

Spike Waveform Classification

Putative inhibitory and excitatory neurons were classified as fast (FS) and regular (RS) spiking respectively, based on the analysis of their spike waveform profile (Sirota et al. 2008; Sakata and Harris 2009; de Souza and Casanova 2019). Prior to the analysis, the temporal resolution was increased using spline interpolation. Two parameters were calculated: The half width of the spike negative deflection and the delay between the negative and the positive peaks (trough-to-peak). Cells were classified in two groups using a K-means clustering algorithm. The validation of the clustering method was performed using the *silhouette* MATLAB (RRID:SCR_001622) function, which calculates an index (silhouette value) ranging from −1 to 1 where values indicate how similar a data point is from its respective group, with negative values indicating a probable misclassified data point. Thus, neurons with negative silhouette values were considered as unclassifiable and were excluded from the analysis (Supplementary Fig. S3).

Statistical Analysis

Statistical analysis was undertaken using the computing environment R (RRID:SCR_001905) with the additional software package PMCMR. Data are expressed as mean ± standard error of the mean (SEM), unless otherwise stated. Data normality was verified using Kolmogorov–Smirnov test. Since data were not normally distributed, different non-parametric statistical approaches were used. Pairwise data comparison was performed using Wilcoxon rank-sum test. Results from LPl and LPm inactivation were analyzed together using Kruskal–Wallis test and Dunn's post hoc with Holm adjustment. Correlation analysis was performed and Pearson's correlation coefficient (r) and significance values are shown. Data obtained from direction tuning curves were compared using the Quade test. The relationship between categories was assessed using Fisher's exact test.

The Network Model

We modeled a layered network of four areas connected feed forwardly, which receive and send additional inputs from and to a parallel structure. The feedforward network (FFN) represents the transmission of visual information throughout the hierarchy of the cat visual cortex. The parallel structure mimics the LP nucleus. The first cortical area receives an excitatory lateral geniculate nucleus (LGN) spiking firing rate input modeled by Poisson spike trains modulated by different contrast levels (see cortical interactions). We considered four levels to mimic processing from areas 17 to 21a, passing across areas 18 and 19. Because we studied the effect of the LP on cortical neurons, for simplicity, we did not consider the direct connection from the LGN to extrastriate cortical areas described in the cat and the feedforward connections from areas 17 to 21a (Wimborne and Henry 1992). Each component of the network consisted of N_E excitatory and N_I inhibitory neurons organized to generate a balanced state. We characterized neurons as $i = 1, 2, \ldots, N_A^\alpha$ of excitatory, E, or inhibitory, I, population, from cortical or thalamic structures ($\alpha = ctx, lp$, where $ctx = 1, 2, \ldots L$ with $L = 4$ and lp as the LP). For each area, including the LP, we simulated $N = 10\,000$ neurons. With such a number of cells, a population of neurons in a balanced regime ensures an asynchronous and stable discharge of neuronal activity. In turn, this asynchronous neural state guarantees a reliable firing rate propagation throughout the network (Vogels and Abbott 2009; Cortes and van Vreeswijk 2015). From this number of neurons, 80% and 75% were excitatory cells from the cortex and the LP, respectively.

We considered an additional 5% of inhibitory neurons in the LP based on available empirical data (Rinvik et al. 1987). This additional 5% produced a slight, but significant increase in thalamic activity, when compared with cortical responses. Both recurrent and afferent connectivity for each layer were random with probability c of connection, in which c is different for E and I populations.

Neuron Dynamics

We used the adaptive exponential integrate-and-fire model (Brette and Gerstner 2005) to describe the dynamics of cortical and thalamic neurons. This neural model consists of two coupled differential equations. The membrane potential of neuron i, of the E or I population A, and cortical or thalamic structure α, were defined by:

$$C_m \frac{dV_i^{A,\alpha}}{dt} = -I_{L,i}^{A,\alpha} - w_i^{A,\alpha} + I_{\text{input},i}^{A,\alpha}, \tag{5}$$

where C_m is the capacitance of the neuron. The first term on the right-hand side of the above equation, given by $I_{L,i}^{A,\alpha} = -g_L^{A,\alpha}(V_i^{A,\alpha} - V_L^{A,\alpha}) + g_L^{A,\alpha}\Delta_T \exp(\frac{V_i^{A,\alpha} - V_T}{\Delta_T})$, consists of a linear component that is the leak current, and a second term that is the exponential function, which characterizes the spike generation process where V_L is the leak reversal potential, V_T is the threshold and Δ_T is the slope factor. The adaptation current, w, obeyed:

$$\frac{dw_i^{A,\alpha}}{dt} = \frac{a(V_i^{A,\alpha} - V_L) - w_i^{A,\alpha}}{\tau_{\text{adapt}}}, \tag{6}$$

where τ_{adapt} is a time constant and a describes the level of subthreshold adaptation. Every time that the neuron i fires, w is increased by a current b (spike-triggered adaptation), and

the membrane potential is reset to a fixed voltage, V_r. Only excitatory neurons have adaptation to current dynamics.

The input current that a neuron $(i,\ A,\ \alpha)$ receives is:

$$I^{A,\alpha}_{\text{input,i}} = I^{A,\alpha}_{rec,i} + I^{A}_{\text{ext,i}}, \tag{7}$$

where $I^{A,\alpha}_{rec,i}$ characterizes the synaptic current from recurrent connections of each area, and the external current, $I^{A}_{\text{ext,i}}$, comprises two or four terms if the unit is from the cortex or the thalamus, respectively.

Recurrent Connections

The recurrent synaptic interactions activate current input to a neuron (i, A, α) as

$$I^{A,\alpha}_{rec,i}(t) = -\sum_{B=E,I} g^{AB}_{i}(t)\left(V^{A}_{i} - V_{B}\right)$$

$$g^{AB}_{i}(t) = \frac{\overline{g}^{AB}_{i}}{\tau^{A}_{syn}} \sum_{j=1}^{N_{ff}} C^{AB}_{ij} \sum_{k} e^{-\left(t-t^{B}_{j,k}\right)/\tau^{A}_{syn}}, \tag{8}$$

where $C^{AB}_{ij} = 0, 1$ is the connectivity matrix, τ_{syn} is the synaptic time constant, and $t^{B}_{j,k}$ is the time of the kth action potential of neuron j of population B and brain region α. So, for simplicity, we assumed an instantaneous rise of the synaptic currents followed by an exponential decay. Recurrent connections were random and the probability varied according to the nature of the cell (i.e., excitatory or inhibitory). The probability of connections was set such as to guarantee that the total number of presynaptic inputs to the neuron $(i,\ A,\ \alpha)$ is on average K. Thus, we requested that the conductance $\overline{g}^{AB}$ is scaled by K as $\overline{g}^{AB} = G_{AB}/\sqrt{K}$, where G_{AB} and K are independent. Thus, the probability of connection was $c_A = K_A/N_A$, for $A = E, I$. This scaling leads to cells to fire close to the maximum rate. However, the strong recurrent connections between excitatory and inhibitory cells balanced each other out leading to a net input on the order of the threshold. Under this regime, without any fine-tuning of parameters, neural populations dynamically arise in the balanced state. As a result, the firing rate of these neurons changes only very weakly if one rescales all the synaptic strengths by the same factor.

Cortical Interactions

Cortical neurons between different areas interacted in a feedforward and a recurrent manner. They received two types of external inputs:

$$I^{A}_{\text{ext,i}}(t) = I^{A,ctx}_{ff,i}(t) + I^{A,lp}_{i}(t), \tag{9}$$

where $I^{A,ctx}_{ff,i}$ is the feedforward cortical input and $I^{A,lp}_{i}$ is the input coming from the LP. Feedforward inputs throughout the chain of cortical areas were defined as $ctx = 1, 2, \ldots, L$. Therefore, the feedforward pathway for the neuron (i, A, ctx) in cortical area $ctx = l$, was defined by the incoming excitatory presynaptic inputs from the previous area $l-1$. Excitatory inputs targeted excitatory and inhibitory populations. Thus, the feedforward input current was defined as $I^{A,ctx}_{ff,i}(t) = -g^{A,l-1}_{ff,i}(t)(V^{A}_{i} - V^{l-1}_{E})$, where the term on the right-hand side of the equation is the sum of all conductances from all presynaptic inputs on neuron $(i, A, l-1)$. It was described as

$$g^{A,l}_{ff,i}(t) = \frac{\overline{g}^{A,l}_{ff}}{\tau^{A}_{syn}} \sum_{j=1}^{N_{ff}} C^{Aff,l}_{ij} \sum_{k} e^{-\left(t-t^{ff}_{j,k}\right)/\tau^{A}_{syn}}, \tag{10}$$

where $t^{ff}_{j,k}$ is the time of the kth spike on neuron (j, ff). The coupling matrices $C^{Aff,l}_{ij}$ for $A = E, I$ and $ff = E$, are random, that is, $C = 1$ with probability $c_{ff}K/N_{ff}$ and $C^{Aff,l}_{ij} = 0$ otherwise. Thus, a neuron (i, A, l) receives, on average, $K_{ff} = c_{ff}K$ inputs from area $l-1$. The conductance $\overline{g}^{A,l}_{ff}$ that describes the weight of the feedforward presynaptic inputs is scaled with K as $\overline{g}^{A,l}_{ff} = G^{A}_{ff}/\sqrt{K}$, where G^{A}_{ff} is independent of K and has equal strength for all cortical areas.

The first cortical area received N_{inp} inputs from a population of LGN excitatory cells. These cells were not modeled explicitly, but they are assumed to have Poisson statistics. The firing rate of an LGN cell (i, ff) depended on the contrast C, which is given by

$$R^{ff}_{i}(C, t) = R^{ff}(C) g_{i}(t), \tag{11}$$

where $R^{ff}(C) = R^{ff}\log_{10}(C+1)$ is the response amplitude due to the visual contrast. The excitatory LGN input, when $l = 1$, to excitatory and inhibitory cortical populations, is modeled with the conductance, $g_i(t)$. $g_i(t)$is the total conductance described in Equation 10, where $t^{ff,0}_{i,j}$ is the time of the jth action potential by neuron (i, LGN), and ff =E.

The other source of external currents to the cortical neurons in area l was the LP. Each cortical area received at the same time inputs from an excitatory population of thalamic neurons. This source of LP neurons was chosen randomly. Therefore, the input current from the LP to cortical neuron (i, A, l) follows$I^{A,l}_{lp,i}(t) = -g^{A}_{ctx\leftarrow lp,i}(t)(V^{A}_{i} - V^{ctx\leftarrow lp}_{E})$, where the term on the right-hand side of the equation is the total conductance of neuron (i, A, l) from all presynaptic LP inputs. Note that we changed $I^{A,lp}_{i} = I^{A,l}_{ctx\leftarrow lp,i}$, to specify the cortical area l that receives inputs from the LP. It obeyed,

$$g^{A,l}_{ctx\leftarrow lp,i}(t) = \frac{\overline{g}^{A,l}_{ctx\leftarrow lp}}{\tau^{A}_{syn}} \sum_{j=1}^{N_{lp}} C^{ctx_A\leftarrow lp_E,l}_{ij} \sum_{k} e^{-\left(t-t^{lp}_{j,k}\right)/\tau^{A}_{syn}}, \tag{12}$$

where $t^{lp}_{j,k}$ is the time of the kth action potential by neuron (j, lp). To avoid confusion, we considered the thalamic conductance such as $g^{A,l}_{ctx\leftarrow lp,i}$for $g^{AB,l}_{i}$, with $B = E_l$ being the excitatory population of neuron from the LP that connects to cortical areal. The connection matrices$C^{ctx_A\leftarrow lp_E,l}_{ij}$, for $A = E, I$, were random with probability $c_{ctx\leftarrow lp}K/N_{ctx\leftarrow lp}$ and $C^{ctx_A\leftarrow lp_E,l}_{ij} = 0$ otherwise. On average, cortical neurons received $K_{ctx\leftarrow lp} = c_{ctx\leftarrow lp}K$ presynaptic connections from LP. Here, the conductance $\overline{g}^{A,l}_{ctx\leftarrow lp}$ describes the strength of the thalamic presynaptic input, which is scaled by K as $\overline{g}^{A,l}_{ctx\leftarrow lp} = G^{A}_{ctx\leftarrow lp}/\sqrt{K}$, where $G^{A}_{ctx\leftarrow lp}$ is independent of K.

Thalamic Interactions

Although the LP receives inputs from subcortical areas (Chalupa et al. 1983), the model considered that the external current for the thalamic neurons depended only on cortical inputs as shown by empirical data (Bender 1983). A thalamic neuron (i, A, lp)

received current inputs simultaneously from the four cortical areas. It obeyed,

$$I^{A}_{ext,i}(t) = \frac{-\sum_{l}^{L} g^{A,l}_{lp\leftarrow ctx,i}(t)}{W(PC,l)}\left(V^{A}_{i} - V^{lp\leftarrow ctx}_{E}\right)$$

$$\bar{g}^{A,l}_{lp\leftarrow ctx,i}(t) = \frac{\bar{g}^{A,l}_{lp\leftarrow ctx}}{\tau^{A}_{syn}} \sum_{j=1}^{N_l} C^{lp_A\leftarrow ctx_E,l}_{ij} \sum_{k} e^{-\left(t-t^{l}_{j,k}\right)/\tau^{A}_{syn}}, \qquad (13)$$

where $t^{lp}_{j,k}$ is the time of the kth action potential of a neuron (j, lp). The weight $W(PC, l)$ scales the input from the cortical layer l to the LP, and it can be independent for each corticothalamic projection. The coupling matrices $C^{lp_A\leftarrow ctx_E,l}_{ij}$, for $A = E, I$, were random, that is, $C = 1$ with probability $c_{lp\leftarrow ctx}K/N_{lp\leftarrow ctx}$ and $C^{lp_A\leftarrow ctx_E,l}_{ij} = 0$ otherwise. On average, thalamic neurons received $K_{lp\leftarrow ctx} = c_{lp\leftarrow ctx}K$ presynaptic connections from each cortex. Here, the conductance $\bar{g}^{A,l}_{lp\leftarrow ctx}$ describes the strength of the cortical presynaptic input, which is scaled by $Kas\bar{g}^{A,l}_{lp\leftarrow ctx} = G^{A}_{lp\leftarrow ctx}/\sqrt{K}$, where $G^{A}_{lp\leftarrow ctx}$ is independent of K.

Parameters

The parameters for the cell dynamics were $Cm = 1\ \mu F/cm^2$, with conductances of leak currents of $g_{L,E} = 0.1\ mS/cm^2$and $g_{L,I} = 0.05\ mS/cm^2$for excitatory and inhibitory neurons, respectively. The other parameters that characterized the dynamic of neurons are: $V_L = -70.6$ mV, $V_T = -50.4$ mV and $\Delta_T = 2$ mV. The parameters for the adaptation current were $a = 24\ nS$, $b = 0.01\ nA$, and $\tau_{adapt} = 60$ ms. For each area, the synapses' parameters were: $G_{E0} = 1.425\ ms\cdot nS/cm^2$, $G_{I0} = 1.89\ ms\cdot nS/cm^2$, $G_{EI} = 9.0\ ms\cdot nS/cm^2$, $G_{II} = 13.5\ ms\cdot nS/cm^2$, $G_{EE} = 22.5\ ms\cdot pS/cm^2$, $G_{IE} = 67.5\ ms\cdot pS/cm^2$, with $\tau_{syn} = 3\ ms$ and $V_E = 0$ mV and $V_I = -80$ mV. Recurrent connectivity for each cortical layer and the LP is $K = 400$, the probability of connection was $c_A = K_A/N_A$, for $A = ff, E, I$.

Variation of Pathway Connections

We used the factors *WFF*, *WCP*, and *WPC* to change the weights of feedforward, pulvino-cortical, and cortico-pulvinar projections. These factors multiply the ratio $G^{\alpha}_{E0}/G^{\alpha}_{I0}$ for those entry inputs. However, for some simulations (Fig. 9, Supplementary Figs S4 and S5), the ratio G^{lp}_{E0}/G^{lp}_{I0} of *WCP* changed across cortical areas to ensure a stable firing rate propagation until the last level of the system. *WPC* was normalized by the number of feedforward areas ($W(PC, l)$, $N = 4$), to avoid an oversaturation of thalamic activity due to an overload of cortical inputs.

Simulations

Network architecture and neuron equations were performed with Python version 3.2 using Brian2 simulator (Stimberg et al. 2014). Euler integration was implemented using a time step of 0.05 ms. The accuracy of the results was verified by repeating simulations with smaller time steps (0.025 ms).

Histology

At the end of the experiment, animals were euthanized with an intravenous injection of sodium pentobarbital (Euthanyl, 110 mg/Kg). Animals were transcardially perfused with a phosphate buffer solution (0.1 M, pH 7.4) followed by a fixative (Paraformaldehyde 4%). Brain tissue was cryoprotected using sucrose solutions at different concentrations (10–30%), frozen and stored at −80 °C. Then, 40 µm coronal sections were obtained and subsequently stained. LP subdivisions were revealed using Acetylcholinesterase staining (Graybiel and Berson 1980). The Chicago Sky Blue staining was used to locate the injection sites and to provide a rough estimation of the extent of the GABA diffusion in the thalamus (Supplementary Fig. S2). Cortical layers were identified using DAPI and the DiI fluorescence signal was used to reconstruct the electrode position. Furthermore, immunostaining of nonphosphorylated neurofilament protein was used to confirm the position of recordings in area 21a (Fig. 5C; Van Der Gucht et al. 2001).

Results

In the present study, from the total number ($N = 1430$) of neurons recorded, 97 (area 17) and 83 (area 21a) units were analyzed. The remaining neurons were discarded due to several factors such as: high response variability, loss of signal during recording sessions, units' failure to recover after the thalamic injections of GABA, or unsuccessful thalamic inactivation. In addition, data from 3 experiments were discarded due to leakage of the GABA injections into adjacent regions of the thalamus. Descriptive statistics (mean, median and SEM values) of all CRF parameters and respective significance levels (P-values) from statistical comparisons are summarized in tables provided as supplementary material.

Effects of LPl Inactivation on the CRF of Area 17 Neurons

The LPl nucleus is the only subdivision of the cat pulvinar that is directly connected to the primary visual cortex in a reciprocal manner (Berson and Graybiel 1983; Casanova 1993). Silencing the LPl yielded changes in the CRF profile of 59 out of 97 areas, 17 neurons (CI overlap mean of 20.96 ± 2.29%). Most changes in the CRF profile were observed at contrast levels >25%. Fig. 2 shows three representative examples of the impact of LPl inactivation on the contrast response of neurons in area 17. In panel A, the LPl inactivation yielded an increase in firing rate (facilitation) of the cortical neuron. This enhancement of activity was observed in 19 units (~32%). Panel B depicts the most frequently observed effect, that is, a decrease (suppression) in the firing rate (37 cells; ~ 63%). Three neurons exhibited a rightward shift of the contrast function (Panel C) and four out of the 19 units showing an increase in firing rate also displayed such rightward shift. In most cases, these changes of activity were not accompanied by significant modification in the cells' preferred orientation and direction and in corresponding tuning functions. Thus, two main groups of cells were identified based on the effect of LPl inactivation: those with facilitated and suppressed responses.

The effects of the LPl inactivation were further characterized by analyzing the parameters of the Naka–Rushton function (eq. 1). Changes on each variable of the equation represented a specific type of gain control of the contrast response curve. Here we identified four contrast-tuning parameters (Fig. 1). The first, contrast gain, is characterized by changes in C50 and represented by a horizontal shift of the curve. The second, response gain, is distinguished by changes of the Rmax and consequently of the contrast curve dynamic range. The third, baseline control, is described by a change in Blsn and represented by a vertical shift of the contrast response curve. Finally, slope control is characterized by changes in the exponential factor (n). In order

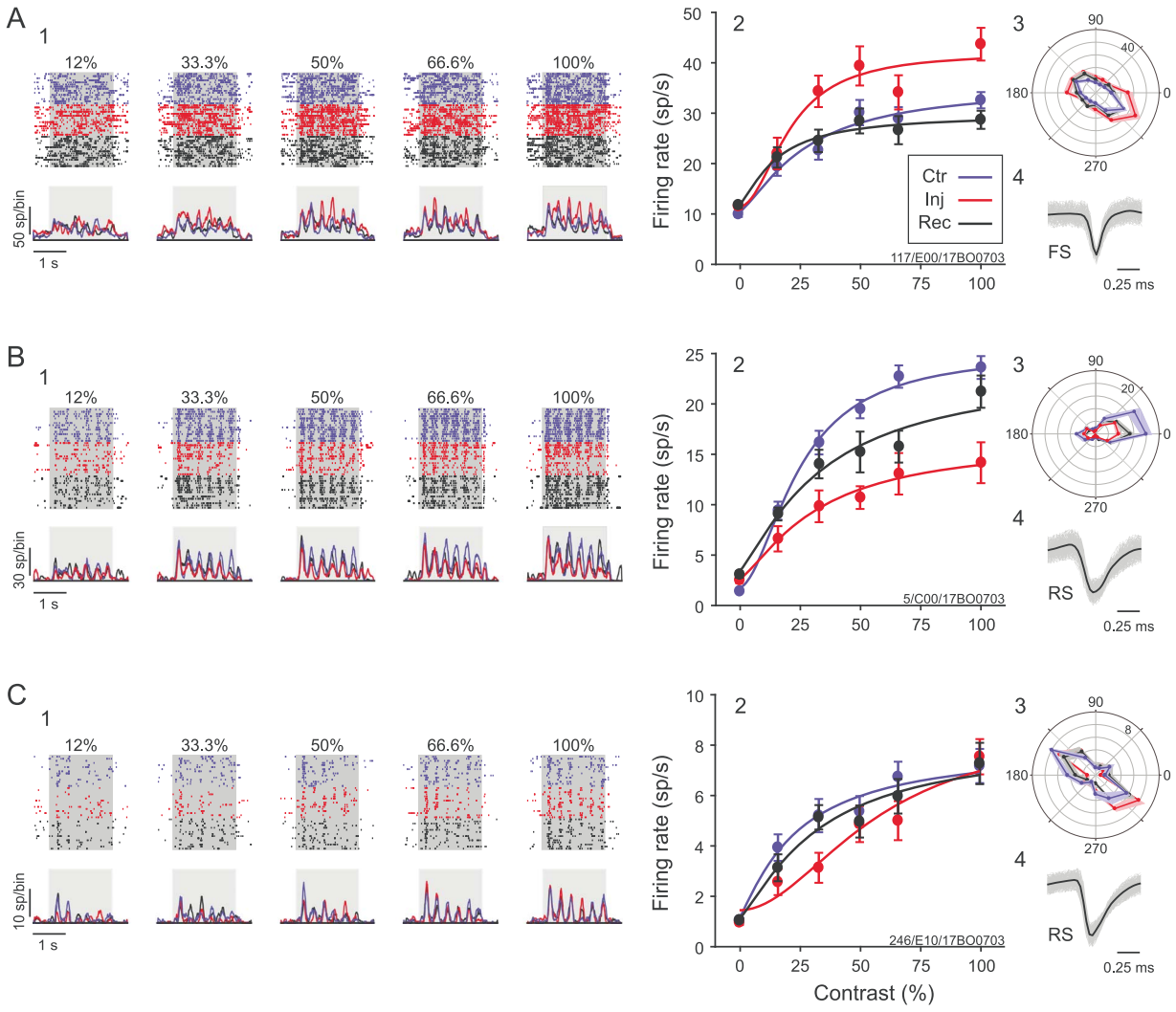

Figure 2. Effects of the reversible inactivation of LPl on the CRF of three neurons from area 17. Neuronal responses during control (blue), thalamic inactivation (red) and recovery (black) are shown. In panels 1–4, Raster plots and PSTHs (1), CRFs (2), direction tunings (3), and spike waveforms (4) are presented for each neuron. (A) The LPl inactivation yielded an increase on the neuron's firing rate at contrast levels higher than 25% (A2). (B) The neuron exhibited a reduction of the firing rate at higher contrast levels (>25%) during LPl inactivation (B2). (C) Here, the LPl inactivation yielded a rightward shift of the neuron's CRF (C2). Note that no changes on the direction selectivity was observed in none of the units shown (Panels 3's). In PSTHs, gray areas represent the duration of the presentation of the visual stimulus (drifting gratings). In CRF plots (panels 2's), dots and error bars represent the average and SEM of neurons' firing rates at different contrasts and lines represent the curve fitting by the Naka-Rushton function. In panels 3's, SEM are represented as shaded areas. In panels 4's, average spike waveforms are depicted as black lines. Ctr = control; Inj = thalamic inactivation; Rec = recovery.

to characterize the type of modulation exerted by the pulvinar, each parameter was compared between control and GABA injection conditions for the 59 areas 17 cells that showed a significant change of activity. Overall, the impact of the LPl inactivation consisted **of** a change in response gain (R_{max}) and baseline control of neurons in the primary visual cortex. Figure 3 illustrates that the neurons in the "facilitated" group exhibited increased response gain and baseline (Panels A and B) while for the "suppressed" group, the LPl inactivation yielded a significant reduction of these two parameters (panels C and D).

Percentage of Variation for the Two Populations in Area 17

The magnitude of the effects of the LPl inactivation was assessed by calculating the percentage of variation (%Var) of the CRF parameters (see Methods for details). Positive and negative %Var values indicate a decrease and increase of a given parameter during inactivation, respectively. Here, we compared the %Var of the CRF parameters between the two previously defined cell groups (facilitated and suppressed) and the total neuronal sample. In accord with the previous analysis, facilitated and suppressed groups exhibited an increase and decrease in the percentage of variation of the response gain and baseline computed from their CRF (Fig. 4).

Effects of LPl Inactivation as a Function of Cortical Depth and Cell Type in Area 17

The %Var of the effects of LPl inactivation on the CRF of area 17 neurons was analyzed as a function of their laminar position, their response modulation to gratings (simple and complex

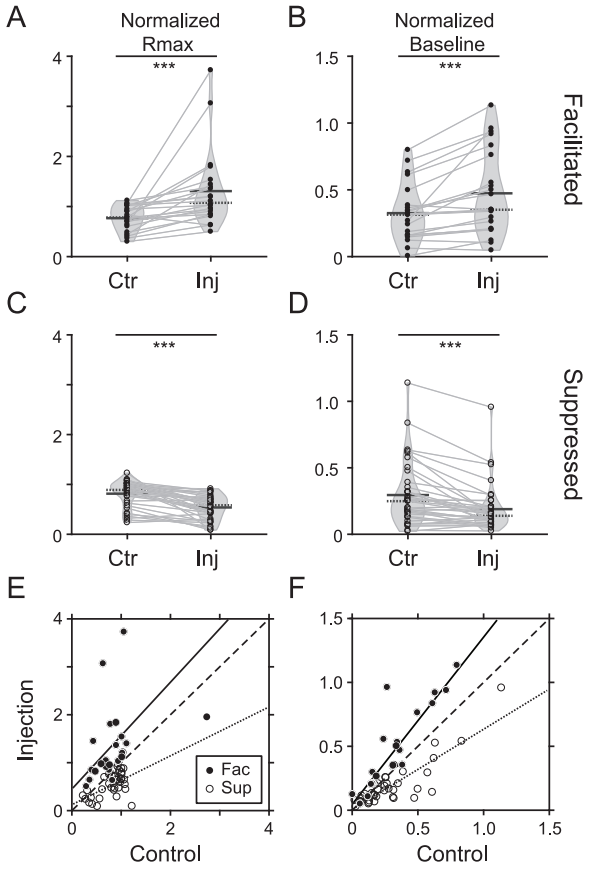

Figure 3. Impact of LPl inactivation on the CRF parameters Rmax and baseline of neurons from area 17. The normalized Rmax and baseline were compared between control (Ctr) and thalamic inactivation (Inj) conditions for two distinct neuronal populations with facilitated (Fac, *A–B*) and suppressed (Sup, *C–D*) responses at high contrast levels during inactivation. Neurons from the facilitated group exhibited an increase in Rmax (*A*) and baseline (*B*) during LPl inactivation whereas those from the suppressed group showed a decrease in both parameters (*C–D*). (*E–F*) Scatter plots of Rmax and baseline of the two groups. Linear regression lines for facilitated (solid line over filled circles) and suppressed (dotted line over empty circles) groups are depicted. For the facilitated group, the regression lines of Rmax ($P = 0.09$, $r2 = 0.13$) and baseline ($P < 0.001$, $r2 = 0.8$) lie above the unity line (dashed line), while the inverse is observed for the suppressed group (Rmax: $P < 0.001$, $r2 = 0.3$; baseline: $P < 0.001$, $r2 = 0.7$). $^{***}P < 0.001$. In *A–D*, solid and dotted lines indicate mean and median values.

cells) and their spike waveform (putative excitatory or inhibitory neurons; Fig. 5; Supplementary Table S3).

Simple versus complex cells. Out of the 59 units analyzed, 39% and 61% were classified as simple and complex cells respectively (Fig. 5*D*). The proportion observed in our study resembles that previously reported in the cat primary visual cortex (Skottun et al. 1991). No differences were observed between simple and complex cells regarding the CRF parameters.

Putative excitatory versus inhibitory cells. From the total number of neurons recorded, 823 units were submitted to the analysis of the spike waveform (Supplementary Fig. S3). From those, a total of 780 units were classified as putative excitatory (72%) and inhibitory (28%) neurons. The proportion of excitatory/inhibitory neurons found in our study agrees with previous observations in cat visual cortex (Gabbott and Somogyi 1986). From the 59 areas, 17 neurons included in the analysis, 32% and 58% were classified as putative excitatory and inhibitory, respectively, while 10% were unclassified (Fig. 5*E*). The difference between the proportion of putative excitatory/inhibitory neurons submitted to spike waveform analysis ($N = 823$) and the subset of units used in the contrast response analysis may be explained by the exclusion of units with low firing rates (see Material and Methods), which favors the selection of inhibitory neurons given their high discharge rates (Wilson et al. 1994; Haider et al. 2006, 2010). The comparison of the CRF parameters between the two neuronal categories revealed that putative excitatory neurons exhibited greater changes in the response gain and slope control in comparison with inhibitory neurons during LPl inactivation (Fig. 5*H,K*). For instance, putative excitatory neurons showed an average decrease of 15.52% while inhibitory neurons showed a slight increase of 0.8% in response gain during inactivation. Similarly, excitatory neurons showed a large increase (17.1%) in the slope while inhibitory neurons exhibited a smaller decrease (6.4%).

Superficial versus Deep Layers . The analysis of laminar position showed that 8.6%, 18.6%, and 72.8% were neurons from layers I/II, III/IV, and V/VI, respectively (Fig. 5*F*). Thus, most neurons were recorded from deep cortical layers (V/VI). This sampling bias was most likely due to the angle of insertion of the probe in the cortex where a larger number of contacts was located in layers V/VI. Therefore, for statistical comparison, neurons were grouped into superficial (I–IV) and deep layers (V/VI). Fig. 5*I* shows that the LPl inactivation tended to preferentially enhance the response gain in the superficial layers while reducing it in the deep layers ($P = 0.07$, Wilcoxon rank sum test).

Finally, we investigated the potential association between the two groups found in area 17 (facilitated and suppressed) and the anatomo-physiological parameters. No significant relationship (Fisher's exact test) was found in any of the parameters indicating that the distinct effects in area 17 induced by the LPl inactivation were independent of the cell type (simple vs. complex; excitatory vs. inhibitory) and its gross laminar position (superficial vs. deep layers).

Effect of LP Inactivation on the CRF of Neurons from Area 21a

In contrast to area 17, area 21a receives direct projections from neurons in the medial and LPl nucleus. Consequently, both subregions were targeted in distinct experiments. Out of the 83 neurons tested in area 21a, 45 and 38 were recorded during the LPl and LPm inactivation experiments, respectively. The evaluation of the CIs overlaps revealed that the inactivation yielded changes in the CRF profile of a large number of cells: 35 out of 45 in LPl experiments and 34 out of 38 in LPm, respectively.

Figure 6 shows four representative examples of the impact of LPl (A–B) and LPm (C–D) on the contrast response of area 21a neurons. For both LPl and LPm experiments, most changes occurred at contrast levels above ~26%. In LPl experiments, the inactivation yielded a facilitation of the visual responses in most neurons (~86%; Fig. 6A–B). For the remaining neurons (5 out of 35), the inactivation yielded a suppression of responses, from which 2 units also exhibited a rightward shift of the CRF. The LPm inactivation also yielded a facilitation of visual responses at higher contrast levels for most units (31 units, ~91%; Fig. 6C–D). However, 11 of these cells also showed a rightward shift of the CRF, and only 3 units (~9%) exhibited suppression in their visual responses during thalamic inactivation. Thus, the inactivation of both LP subdivisions yielded more homogenous effects on

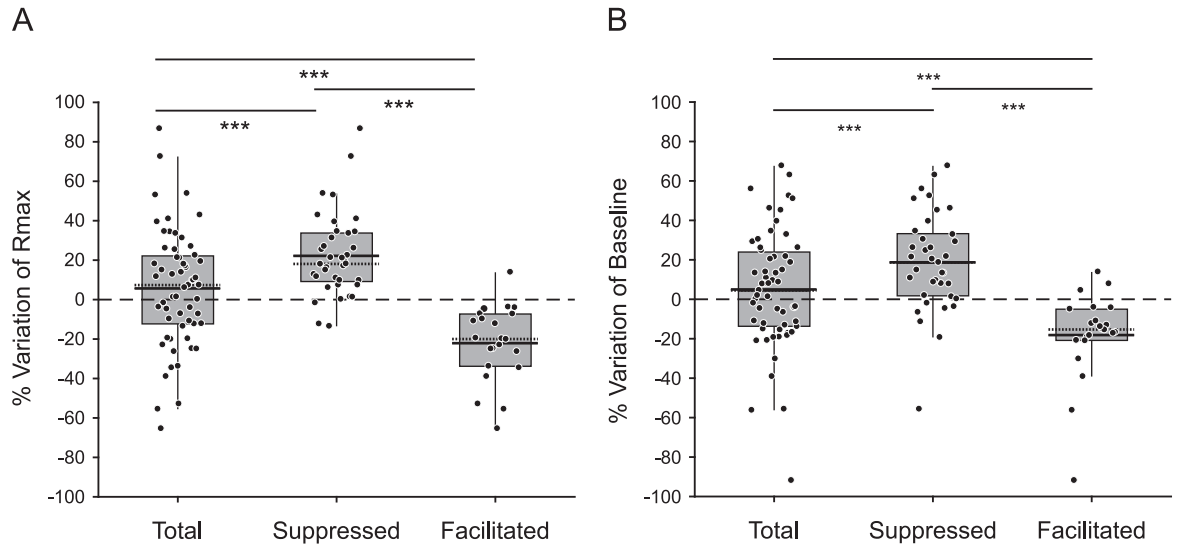

Figure 4. Comparison the percentage of variation (%Var) of the CRF parameters Rmax and baseline of neurons from area 17. Here, the total population is compared with the facilitated and suppressed groups. (*A*) %Var of Rmax. **On average**, facilitated neurons exhibited negative %Var values indicating an increase in the CRF response gain during LPl inactivation. **In contrast**, suppressed neurons showed positive %Var values representing a decrease of the CRF response gain. The pooled dataset (Total) exhibited a slight decrease of the CRF response gain as a smaller average positive Rmax %Var value. (*B*) %Var of the baseline. As for the Rmax, facilitated neurons exhibited negative %Var values while the suppressed group showed positive values indicating a decrease and increase of baseline levels, respectively. The total population exhibited small positive %Var baseline values indicating a slight decrease on this parameter. In boxplots, solid and dotted lines indicate mean and median values, respectively. ***$P < 0.001$.

the CRF of 21a neurons than those observed in area 17 after LPl inactivation and these effects were mainly characterized by a response facilitation.

Next, the effects of the inactivation of both subdivisions were further characterized by analyzing the CRF parameters (Supplementary Table S4). Figure 7 shows the main effects of LPl and LPm inactivation on the contrast response of 21a neurons. The LPl inactivation yielded an increase in response gain and baseline (panels *A–B*). As in LPl experiments, the main effects of LPm inactivation consisted **of** increases in response gain and baseline (panels *C–D*). In addition, the LPm inactivation yielded an increase in the contrast gain (C50) and a reduction in the curve slope.

Effects of LP Inactivation in Function of Cortical Depth and Cell Type of Area 21a Neurons

Out of the 69 neurons analyzed, most were complex-like ($N = 66$) with only three were classified as simple-like cells. This proportion is in accordance with previous reports showing that most area 21a neurons have complex-like receptive fields (Wimborne and Henry 1992; Dreher et al. 1993; Tardif et al. 1996). Regarding the other properties, the percentage of variation (%Var) of the CRF parameters of 21a neurons were compared in the function of the cell type (putative excitatory vs. inhibitory cells; Supplementary Table S5) and laminar position (superficial vs. deep layers; Supplementary Table S6).

Putative excitatory versus inhibitory cells. The spike waveform analysis revealed that 37 and 23 neurons were classified as putative excitatory (RS) and inhibitory (FS) cells, respectively. In LPl experiments, the proportion of putative excitatory and inhibitory cells was ~43% (15 units) and ~57% (20 units), while in LPm, they composed ~86% (22 units) and ~12% (3 units) of the sample, respectively. Due to the low number of FS neurons recorded during LPm inactivation ($N = 3$), no statistical analysis was performed. Regarding the LPl experiments, the CRF slope of excitatory and inhibitory neurons was distinctively affected during inactivation ($P = 0.02$, Wilcoxon rank sum test) where excitatory neurons showed a larger decrease (31.26% vs. 0.37%).

Superficial versus deep layers. In LPl experiments, ~17% and ~83% were from layers III/IV and V/VI, respectively. In LPm experiments, ~10%, ~31%, and ~59% were neurons from layers I/II, III/IV, and V/VI, respectively. The same sampling bias observed in area 17 was thus also present here, where neurons from deep layers were more represented in the sample. Thus, for statistical comparison, we grouped the neurons in superficial (layers I–IV) and deep (layer V/VI) layers.

Neurons from superficial and deep layers were distinctively impacted by LPl inactivation. Differences were observed in the response gain and slope control. For instance, the LPl inactivation yielded an average increase of the response gain in both superficial (%Var R_{max} mean of $-46.55\% \pm 9.28$) and deep layers (%Var R_{max} mean of $-9.71\% \pm 5.05$), but with more pronounced effect in the former (by a factor of 4.8 times; $P < 0.01$, Wilcoxon rank sum test). In addition, neurons from superficial layers exhibited a more pronounced decreased in the CRF slope (%Var n mean of $50.22\% \pm 12.74$) in comparison with neurons from deep layers (%Var n mean of $6.03\% \pm 8.01$; $P < 0.05$, Wilcoxon rank sum test). In contrast to the above observations, there was no relationship between the changes in response and the laminar position of the cells when the LPm was inactivated.

Comparison of LP Effects across Cortical Areas

The amplitude of the effects of thalamic inactivation between areas 17 and 21a was assessed by comparing the %Var of the CRF parameters. Since our goal was to evaluate the global impact of thalamic inactivation on both cortical areas (LPl for areas 17 and 21a; LPm for area 21a only), in this analysis, the total sample from area 17 was considered. In area 17, the net impact of LPl inactivation was characterized by a small decrease in the response gain and baseline. Conversely, in area 21a, the LPl

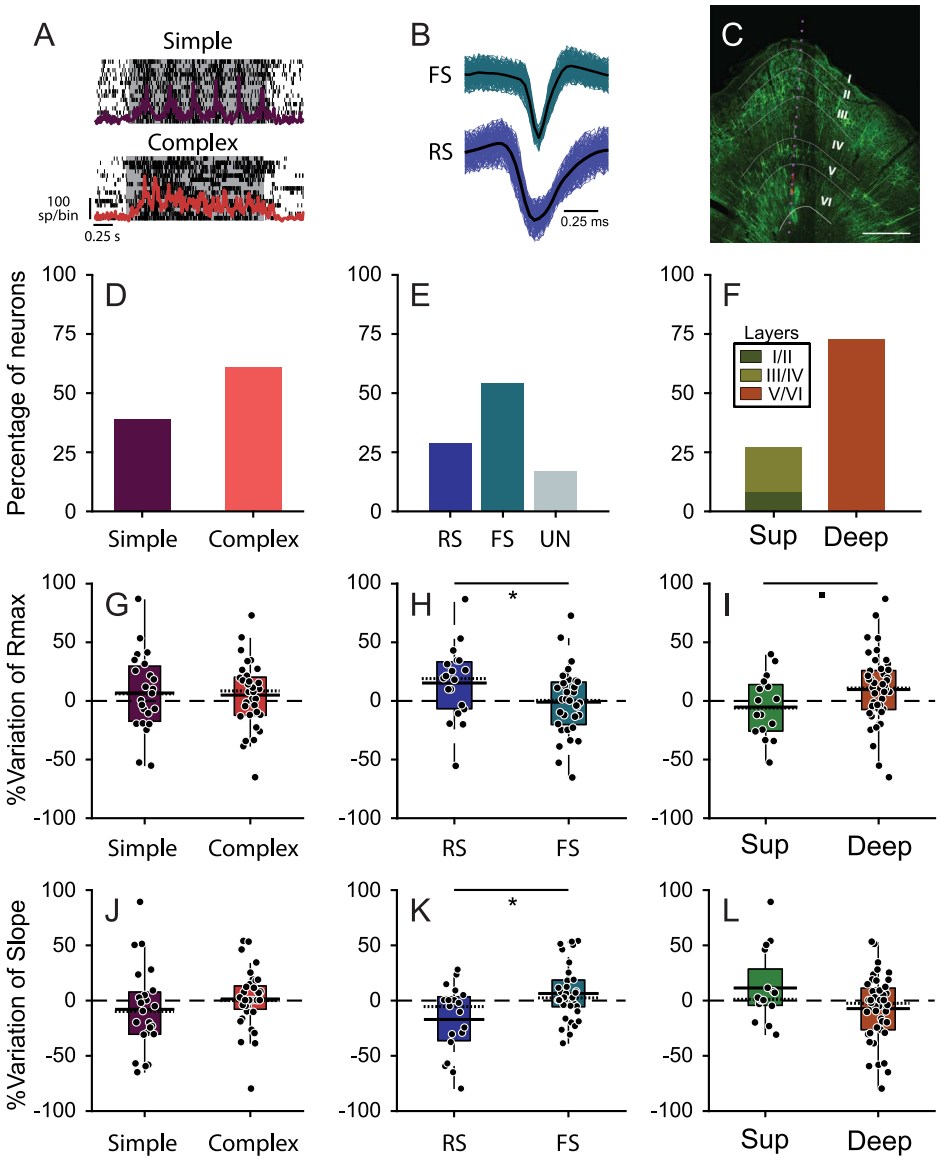

Figure 5. Comparison the percentage of variation (%Var) of Rmax and slope of neurons from area 17 in function of their physiological properties and cortical laminar position. Data were compared between simple and complex cells (*A*, *D*, *G*, *J*), putative excitatory (regular spiking) and inhibitory (fast-spiking) cells (*B*, *E*, *H*, *K*) and cortical laminar position (*C*, *F*, *I*, *L*). (*A*) PSTH and raster plots of a simple and a complex cell. (*B*) Spike waveforms of a regular spiking (RS) and a fast-spiking (FS neurons. (*C*) Reconstruction of recording contacts (magenta dots) across the cortical depth of area 17. D-F) Proportion of neurons in the different categories compared. (*G–I*) %Var plots for Rmax. In H, RS neurons were more impacted by LPl inactivation exhibiting a decrease in the response gain (i.e., positive %Var valuess). In *I*, there was a tendency that neurons from deep layers exhibiting an average decrease in the response gain as well. (*J–K*) %Var plots for slope. UN = unclassified, Sup = superficial layers. ■ $P < 0.1$, $^*P < 0.05$. IN boxplots, solid and dotted lines indicate mean and median values, respectively. In *A*, shadowed regions indicate the duration of the stimulus presentation (drifting gratings).

yielded a larger increase of response gain and baseline (Fig. 8). However, the LPm inactivation yielded even larger changes on response gain and baseline. For instance, the average %Var of response gain during LPm inactivation was ~2.7 and ~7.7 times larger than those induced by LPl inactivation on area 21a and 17, respectively. Additionally, the increase of the baseline was ~2.97 and ~7.27 times larger than that observed in area 21a and 17 during LPl inactivation, respectively.

Modeling the Transthalamic Pathway

Our experimental data showed that the main impact of the LP inactivation in the CRF of areas 17 and 21a was characterized by small decreases and large increases in the response gain, respectively. Here, we created a theoretical model in order to mimic those effects. The theoretical cortical visual system was simulated by a network of four layers connected in a feedforward way with excitatory inputs (FFN). The LP was represented by an external and parallel population of neurons interacting with the FFN through reciprocal excitatory connections (Fig. 9A). The first area of the network received an external input mimicking the LGN projections. The LGN firing rate consisted **of** uncorrelated Poisson excitatory spikes that varied logarithmically with contrast. This signal mimicked the visual contrast used in our experiments. This arrangement of connections between areas

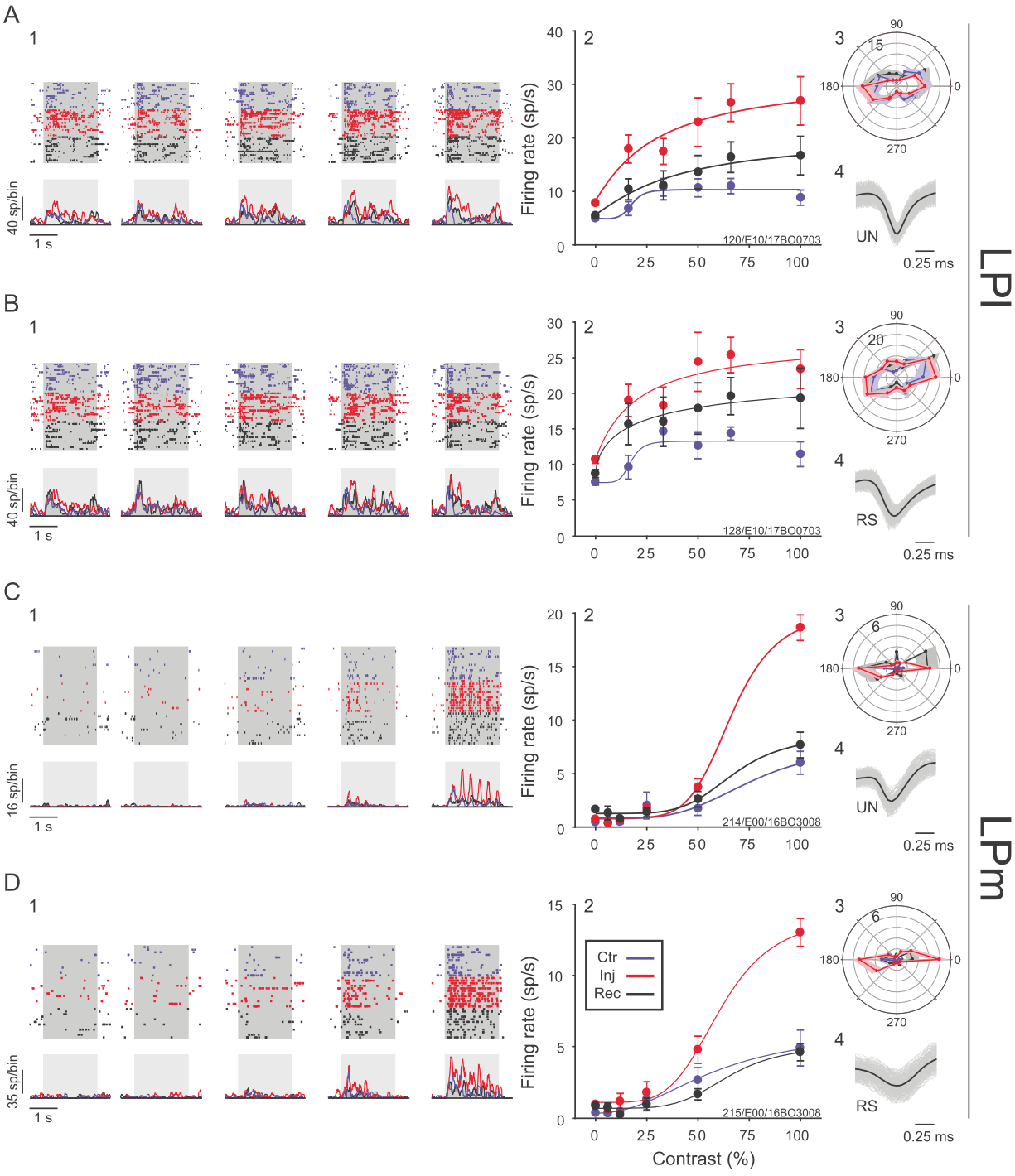

Figure 6. Effects of the reversible inactivation of LP on the CRF of four neurons from area 21a. (A–B) Examples of the effects of the inactivation of the lateral LP subdivision (LPl). (C–D) Examples of the impact of the medial LP (LPm) inactivation. Note that the main impact in both subdivisions was an increase in the firing rate at high contrast levels (Panels 2's) with a larger impact during LPm inactivation (C2 and D2). No changes on the direction selectivity were observed (Panels 3's). The same layout from Figure 2 is applied here. RS = regular spiking; UN = unclassified.

allowed a stable propagation of the signals across the FFN. For instance, in each level of the FFN, the activity increased in the function of the contrast mimicking the CRF (Fig. 9B). This was previously observed in other theoretical studies proposing that the pulvinar allows a stable propagation of visual signals across the cortex preserving the contrast sensitivity at higher levels of the hierarchy (Cortes and Van Vreeswijk 2012; Cortes and van Vreeswijk 2015).

After creating the corticothalamic system, the GABA injection in LP was simulated as a global reduction of its connectivity strength (50% of the initial strength). The robust recurrent connectivity between excitatory and inhibitory neurons produced

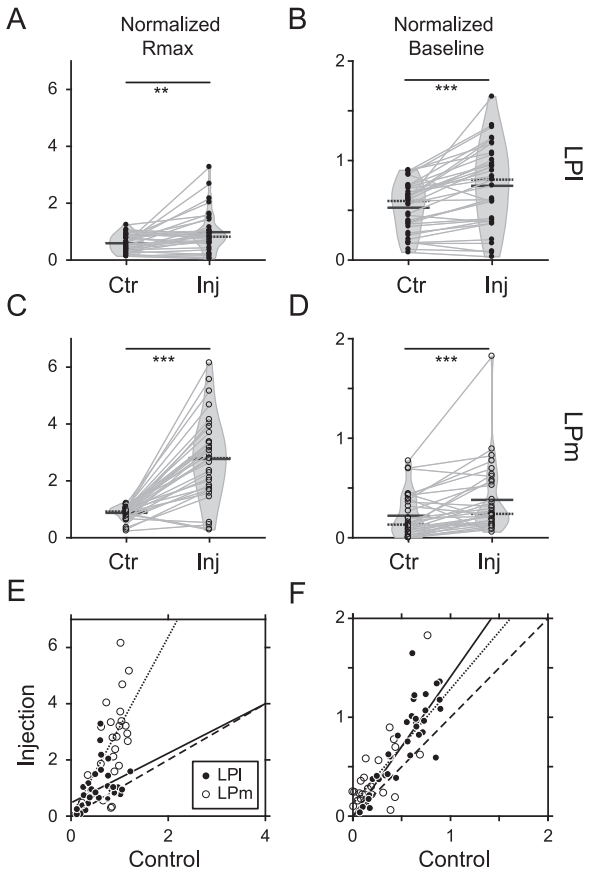

Figure 7. Impact of LP inactivation on the CRF parameters Rmax and baseline of neurons from area 21a. The normalized Rmax and baseline were compared between control (Ctr) and thalamic inactivation (Inj) conditions during inactivation of the LPl (*A–B*) and LPm (*C–D*). The LPl inactivation yielded an increase in Rmax (*A*) and baseline (*B*). In comparison, the inactivation of the medial LP subdivision (LPm) yielded a greater increase in Rmax (*C*) and a similar increase in the baseline (*D*). *E–F*) Scatter plots of Rmax and baseline of LPl (filled circles) and LPm (empty circles) inactivation. Note that most of data points and of both groups were located above the unity line (dashed line) showing an increase in Rmax (linear regression LPl: $P < 0.05$, r2 = 0.13; LPm: $P < 0.01$, r2 = 0.29) and baseline (linear regression LPl: $P < 0.001$, r2 = 0.72; LPm: $P < 0.001$, r2 = 0.52). The same layout from Figure 3 is applied here. $^{**}P < 0.01$, $^{***}P < 0.001$.

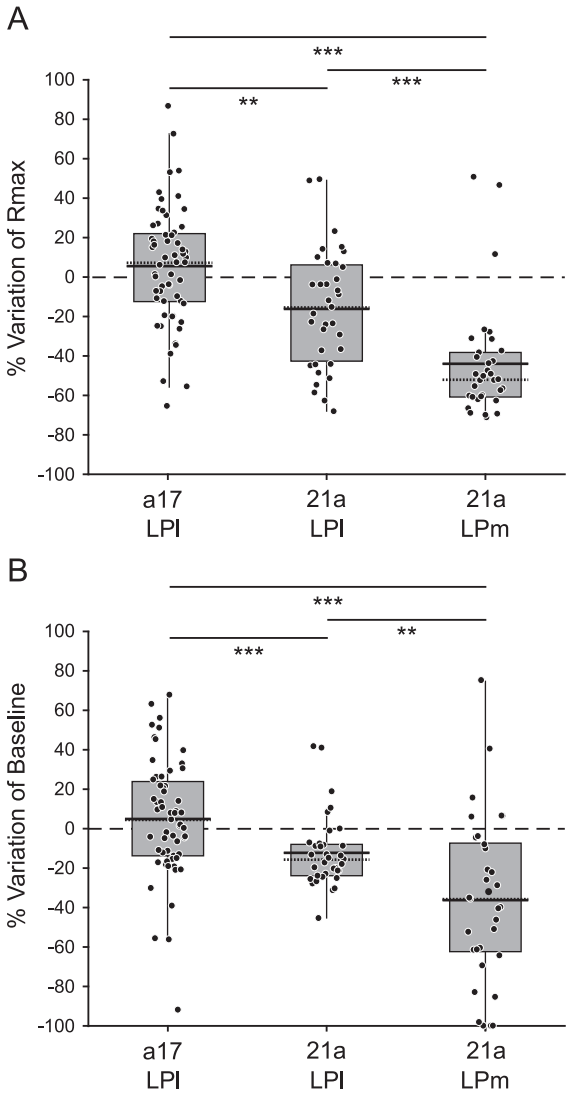

Figure 8. Comparison the percentage of variation (%Var) of Rmax and baseline between area 17 and 21a during LP inactivation. The net effects of LPl and LPm inactivation on areas 17 and 21a were compared. (*A*) Rmax %Var. In area 17, LPl inactivation yielded a small positive Rmax variation while in area 21a, both LPl and LPm inactivation yielded stronger negative variations of this parameter. Thus, the effect of LPl inactivation was a slight decrease in the CRF response gain in area 17 whereas in area 21a, an increase was observed. (*B*) Baseline %Var. Similarly, LPl yielded a slight positive change in the baseline %Var in area 17, while in area 21a, LPl and LPm inactivation yielded a larger negative change in this parameter. Note that the largest changes on both Rmax (*A*) and baseline (*B*) were observed in area 21a during LPm inactivation. Solid and dotted lines indicate mean and median values, respectively. $^{**}P < 0.01$, $^{***}P < 0.001$.

a net increase of the LP output firing rate at higher contrast levels. Then, the effects of the GABA injection with LP-cortical projections targeting either excitatory or inhibitory cortical populations were assessed (Supplementary Fig. S4). First, excitatory neurons of the FFN received LP projections with equal strength of connectivity. During the control period, the neuronal activity was transmitted nonlinearly throughout the visual cortex, creating a stair-shaped CRF in the last area (S4A). This unrealistic response was avoided by gradually increasing the strength of LP connections from the first to the last cortical area. Here, the dynamic range of cortical areas showed a greater increase during LP inactivation than during control periods (Supplementary Fig. S4B). In contrast, when only inhibitory neurons were targeted, the CRF dynamic range decreased during LP inactivation (Supplementary Fig. S4C,D). Interestingly, as revealed in our experimental findings, the neurons' CRFs were modulated mostly at high contrast levels. Indeed, the CRF in all cortical areas were scaled up or down when excitatory or inhibitory neurons were targeted mimicking the response gain control observed in the present study. The model produced these results when the cortico-LP connectivity strengths were weak while the LP-cortical ones were strong. In this setting, the LP controlled the cortical response gain, as previously described (Cortes and Van Vreeswijk 2012; Cortes and van Vreeswijk 2015). Next, another scenario was created, in which the LP-cortical inputs targeted both excitatory and inhibitory cortical populations (Fig. 9). Here, the weights of LP-cortical connections targeting inhibitory populations were equal for each cortical area while the weight of connections targeting excitatory populations was progressively

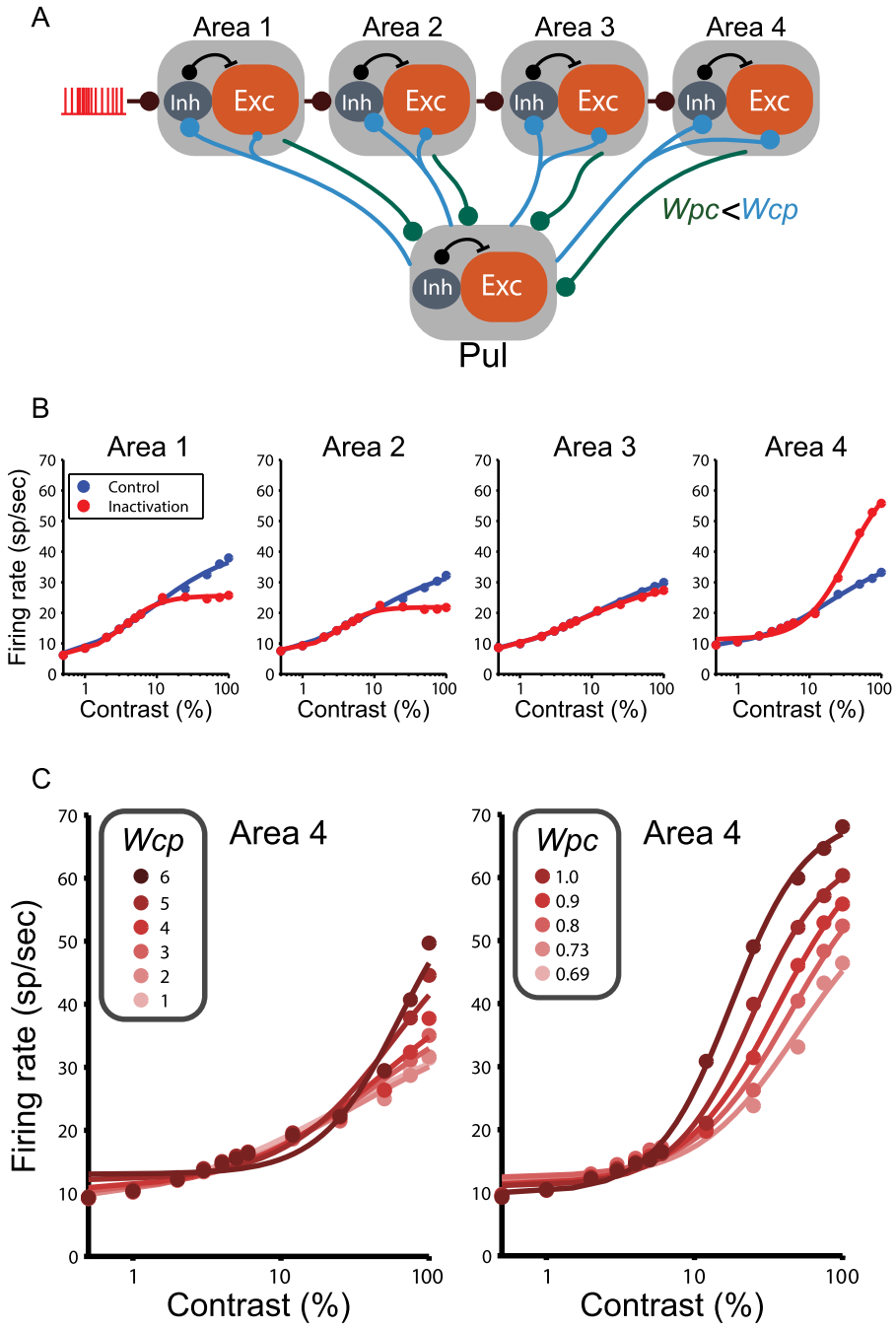

Figure 9. Modeling the transthalamic pathway. (*A*) Model of a layered FFN of four areas connected reciprocally to an external structure (pulvinar). Each area of the model, including pulvinar, consists of excitatory and inhibitory neurons connected strongly to reach the balanced state. The input to area 1 is K = 400 excitatory uncorrelated Poisson spikes. The excitatory population of one area connects homogeneously in a random manner the neurons of the next area. The feedforward connections have on average K numbers of synapses, with equal strength of connectivity (W_{FF}) across the four areas. Pulvinar receives and sends excitatory projections from and to the FFN, with weights W_{PC} and W_{CP}, respectively. Note, however, that the excitatory connectivity from the pulvinar to the excitatory neurons in area 1 is weaker than the connectivity to the excitatory population in the last area. (*B*) Firing rate as a function of contrast for the four cortical areas. Dots represent simulation results for control (blue) and inactivation (red) conditions. Solid lines are fits of CRFs. Note that the first area decreases and the last increases its firing rate during inactivation. Inactivation consists of a reduction of pulvinar internal weights by 25%. (*C*) Left graph shows firing rate of last area when pulvino-cortical weights (W_{PC}) increase while magnitudes of cortico-pulvinar connections remain fixed (W_{CP} = 0.6). Right graph shows firing rate of last area when pulvino-cortical weights (W_{PC}) increases and W_{PC} = 4. The 2 sets of simulations have equal cortico-cortical strength of connectivity (W_{FF} = 10).

increased across the FFN (Fig. 9A). This solution was found when LP-cortical weights were stronger than the cortico-LP ones. This possible solution is supported by our experimental findings where both putative excitatory and inhibitory neurons were impacted by LP inactivation, but with greater effects observed in excitatory neurons.

In the above-mentioned solutions, the simulation of the GABA injections yielded a net increase of the LP output. In

order to mimic a decrease of the LP output firing rate, only the weights of inhibitory connections were reduced (50% decrease of initial strength). In this setting, the weights of LP-cortical inputs targeting excitatory populations were the same across the cortical areas while the weights to inhibitory populations gradually increased from the first to the last area. In addition, the LP-cortical weights were weaker than the cortico-LP ones. In this setting, a qualitatively similar solution was obtained where the LP inactivation yielded a decrease and an increase of the response gain in the first and last cortical areas (Supplementary Fig. S5). However, in this case, our model could not mimic the greater increase of the response gain at the last cortical area.

In our simulation, the LP inactivation resulted in a decrease and increase of the firing rate at high contrast levels in the first and last areas of the FFN, respectively. The progressive increase of the weights of LP-cortical connections on the FFN induced a considerable increase of the firing rate in the last area of the chain, mimicking the increased response gain shown by neurons in area 21a (Fig. 9*B*). Thus, our model supports the notion that the LP controls the contrast response in areas 17 and 21a by modulating the excitatory and inhibitory inputs in a balanced way (Abbott and Chance 2005), characterized by changes in the response gain rather than a contrast gain. None of the solutions proposed in our theoretical model showed changes in the contrast gain, as observed in neurons from area 21a during LPm inactivation.

Discussion

In this study, we investigated the impact of the reversible pharmacological inactivation of the LP nucleus on the contrast response of neurons in a low (area 17) and a higher-level area of the cortical hierarchy (area 21a). Our findings demonstrated that LP inactivation yielded distinct changes on the CRF of cortical neurons. In area 17, the main impact of LPl inactivation on the neurons' CRFs was characterized by a small decrease in the response gain. Conversely, in area 21a, the LPl inactivation yielded a more pronounced increase in the neurons' response gain. During LPm inactivation, changes were observed in all CRF parameters of 21a neurons with a strikingly large increase in the response gain and an increase in contrast gain, baseline and a reduction in the slope.

The area 21a is placed at a higher level in the cortical hierarchy in relation to area 17 and is considered as a gateway area of the cat ventral stream (Payne 1993; Scannell et al. 1995). Several distinctions are also observed at a functional level where the response profile of 21a neurons is more similar to LP neurons (e.g., binocularity and complex-like RFs) than to those from area 17 (Tardif et al. 1996; Vickery and Morley 1999). Thus, to obtain comparable measures of the effects of the thalamic inactivation, it was imperative to use a visual stimulus that reliably elicits a neuronal response in both cortical areas. In the present study, drifting gratings with varying contrasts were found to be a suitable stimulus as neurons from both cortical areas were sensitive to contrast changes. Indeed, contrast sensitivity is observed in several areas across the visual system (Enroth-Cugell and Robson 1966; Tardif et al. 1996; Avidan et al. 2002; Burkhardt 2011) and, with some exceptions (Sani et al. 2013), the contrast response is stereotypically described as a sigmoidal curve better characterized by a hyperbolic function (Naka and Rushton 1966). Here, the responses of neurons from both cortical areas were well fitted by the Naka–Rushton function that allowed us to characterize, quantify, and compare the distinct types of gain control of the CRF during thalamic inactivation.

The CRF as a Measure of the Nature of Thalamocortical Projections

Projections to and from distinct thalamic nuclei involved in visual, auditory, and somatosensory processing were previously characterized based on their anatomical and physiological properties (Sherman and Guillery 1996; Reichova and Sherman 2004; Lee and Sherman 2008; Ji et al. 2016). Two main categories were identified: drivers and modulators. Driver inputs carry the main message while modulators modify that message (Sherman and Guillery 1998). Alternatively, drivers and modulators can be distinguished based on how the excitatory and inhibitory inputs are integrated affecting a neuron's firing rate (Chance et al. 2002; Abbott and Chance 2005). In this classification framework, a driver control is characterized by a push–pull mechanism between excitatory and inhibitory inputs (Anderson et al. 2000) while a modulatory effect occurs by the combination of both input types in a balanced mode (van Vreeswijk and Sompolinsky 1996; Chance et al. 2002). Indeed, theoretical and experimental data have shown that push–pull excitation and inhibition yield additive/subtractive effects in a neuron's firing rate (Gabbiani et al. 1994; Anderson et al. 2000). On the other hand, multiplicative/divisive changes of a neuron's firing rate occur when the level of balanced inputs (i.e., combined excitatory and inhibitory signals) is modified (Chance et al. 2002; Abbott and Chance 2005). Here, we applied this principle to the interpretation of the effects of LP inactivation on the contrast response curve. For instance, additive/subtractive changes of the CRF are translated by changes in the contrast gain and baseline control while multiplicative/divisive effects are observed as changes in the response gain and slope control (Fig. 1). Thus, based on this interpretation, we observed that the LP inactivation yielded mainly modulatory effects on the CRF of areas 17 and 21a. However, one may propose that changes to the CRF of cortical neurons cannot be exclusively attributed to either a driver or a modulatory influence from the pulvinar. Indeed, previous studies have demonstrated that the contrast response of cortical neurons is strongly influenced by the local network (Soma et al. 2013) as well as by long-range sources as those involved in attentional modulation of visual processing (Ling and Carrasco 2006; Williford and Maunsell 2006; Cutrone et al. 2014). Thus, one cannot rule out the possibility that other processes have influenced the CRF of cortical neurons in our study, especially in area 21a, as evidence suggests that the impact of modulatory mechanisms, such as attention, increases as a function of the visual hierarchy (Goris et al. 2014).

The Nature of LP Inputs in the Primary Visual Cortex

Our findings showed that the influence of LPl on neuronal responses in area 17 was mostly modulatory, as revealed by an increase (facilitated group) and a decrease (suppressed group) in the response gain during inactivation. In a study aimed at determining the impact of pulvinar on oscillatory activity in the cat (Molotchnikoff and Shumikhina 1996) reported increased and decreased responses to high contrast (50% and 80%) drifting gratings during LPl inactivation. These changes can be explained by the modulation of the CRF response gain observed in the present study. In primates, the visually evoked and sponta-

neous activity of neurons from area 17 supragranular layers was strikingly reduced during pulvinar inactivation (Purushothaman et al. 2012). These results suggest that the pulvinar would be essential for the activity of neurons in this region, which can be interpreted as a driver input. Our findings are at odds with this assumption since the impact LPl inactivation was almost exclusively modulatory as shown by the effects on the response gain. Previous theoretical studies have investigated the potential role of the pulvinar in visual cortical circuitry (Crick and Koch 1998; Cortes and Van Vreeswijk 2012; Cortes and van Vreeswijk 2015). For instance, Crick and Koch (1998) proposed the so-called "no-strong-loop" hypothesis, which predicts that two reciprocally connected areas cannot drive each other, which otherwise would inevitably cause the system to oscillate uncontrollably. Based on this hypothesis, since LPl receives its main driving inputs from area 17 (Abramson and Chalupa 1985; Chalupa and Abramson 1989; Casanova et al. 1997), it would be unlikely that the thalamocortical projections would be a driver in nature. Indeed, the theoretical model shows that decreased connectivity strength of the pulvinar toward the first cortical area is essential to obtain a balanced change of the neuronal response in function of the visual contrast. Thus, our model corroborates our experimental data indicating that the nature of pulvinar inputs to area 17 is modulatory.

The Nature of LP Inputs in Area 21a

Our experimental findings demonstrated that the LP nucleus exerts a stronger modulatory influence on area 21a than on area 17. These results are supported by our mathematical model, which shows that thalamocortical connectivity should be stronger in higher areas than in areas located at lower hierarchical levels (Fig. 9). Previous studies indicated a modulatory role of pulvinar on higher-order cortical areas. For instance, in the primate area V2, Soares et al. (2004) showed that the pulvinar inactivation yielded an increase in the neurons' spontaneous activity and visual responses. Here, we provided evidence that these effects may originate from changes in baseline and response gain of cortical neurons. In cats, a previous study from our group (Minville and Casanova 1998) showed that the LPl inactivation had a small impact on the basic properties of neurons from the PMLS area (e.g., spatial frequency and direction tunings), an extrastriate area from the cat dorsal stream (Dreher et al. 1996). Thus, one may conclude that the LP does not participate **in** the creation of basic properties in this higher-order visual area, therefore in agreement with a modulatory rather than a driver input. Similarly, our results showed that LPl exerts a modulatory influence on the contrast processing in area 21a. The modulatory nature of the LP input to area 21a was not expected since most projections end in layer IV and thus, be considered as drivers, that is, contributing to basic receptive field structure of neurons (Felleman and Van Essen 1991; Jones 2001; Sherman and Guillery 2013). This suggests that the general scheme of an organization described along the geniculo-cortical pathway may not be applied to extrageniculate pathways. Indeed, it is well known that LGN neurons reaching layer IV provide a driver input to the primary visual cortex (Kandel and Schwartz 2013; Sherman and Guillery 2013); however, nothing is black and white here. Although the main influence of LPm on area 21a was modulatory (as for LPl), characterized by an increase in the response gain, a driver component was equally present since an increase in the contrast gain was also observed (Fig. 10). Although

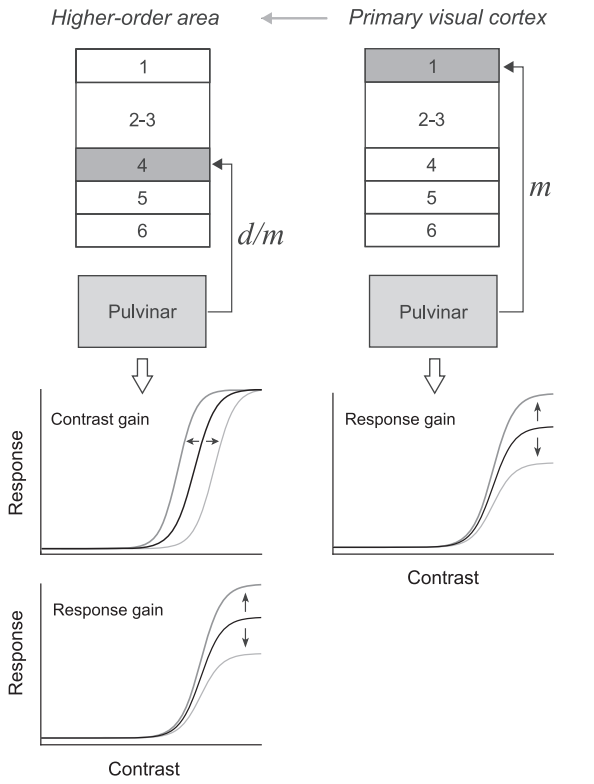

Figure 10. Scheme of the nature of pulvino-cortical connections with the primary visual cortex and an extrastriate area based on our findings. The hypothetical scheme shown in Figure 1 is updated here taking into account our findings. The prediction made for the nature of pulvino-cortical inputs in the primary visual cortex (e.g., area 17) was confirmed indicating that it is mostly modulatory. This was exemplified in our study mainly by non-linear changes (i.e., response gain) in the CRF of neurons from area 17 during LPl inactivation. On the other hand, the impact of LP (LPl and LPm) inactivation was mostly characterized by changes on the response gain and contrast gain of the CRF of neurons from area 21a. This indicates that the pulvino-cortical projections exert both a modulatory (LPl) and driver (LPm) actions on the neuronal activity in a higher-order area from the ventral stream (area 21a), challenging our initial predictions (see Fig. 1).

the weight of the LP signals remains to be determined to identify its driver/modulatory nature, our mathematical model suggests that the thalamic projections are weaker than the feedforward cortico-cortical pathway (Fig. 9). The notion that the driver cortico-cortical feedforward connections exert a stronger impact in area 21a than that of the thalamocortical projections is supported by previous studies suggesting that the former is essential for the maintenance of the contrast sensitivity in the cortical network (Litvak et al. 2003; Kumar et al. 2010; Cortes and van Vreeswijk 2015).

Although both lateral and medial subdivisions of the LP are connected to area 21a, they receive their main excitatory inputs from area 17 and superior colliculus, respectively (Berson and Graybiel 1983; Raczkowski and Rosenquist 1983; Abramson and Chalupa 1985). Therefore, distinct neuronal properties are observed between the LP subdivisions, which resemble their respective main inputs (Chalupa et al. 1983; Chalupa and Abramson 1989; Casanova et al. 1997). Interestingly, the distinct effects of the inactivation of the two LP subdivisions on the CRF of area 21a neurons may reflect their respective functional roles. For instance, the predominantly modulatory inputs from LPl may be related to the modulation of the processing of visual

information through the transthalamic pathway. On the other hand, the presence of driving components in the LPm inputs may be related to the processing of visuomotor signals originated from the superior colliculus.

Functional Implications of the Role of the Pulvinar on Cortical Processing

Our findings showed that the LP exerts distinct modulatory influences on the contrast processing in areas 17 and 21a. In addition, the stronger impact of LP inactivation in area 21a suggests that the pulvinar may play a more important role on visual processing at higher levels of the cortical hierarchy. What mechanisms could underlie these distinct effects? In our theoretical model, differences in the target population as well as in the strength of thalamocortical connections could represent a possible mechanism for the distinct effects of LP inactivation on the visual cortex. Our simulation strongly suggests that the LP regulates cortical contrast responses by a gain control mechanism based on the variation of the balanced forces between excitatory and inhibitory cortical populations (Abbott and Chance 2005; Cortes and van Vreeswijk 2015). Thus, our experimental and theoretical data support the notion that the pulvinar impact on the visual processing at higher levels of the cortical hierarchy is mostly modulatory.

Our current experimental results suggest that the LP is involved in the transmission of information by modifying the representation of the visual contrast throughout the visual cortex. This effect is illustrated by the increase in the response gain of neurons in area 21a during LP inactivation (Fig. 6), a prediction that was addressed by previous theoretical works (Cortes and Van Vreeswijk 2012; Cortes and van Vreeswijk 2015). However, those models did not predict the decreased and increased response gain in areas 17 and 21a, respectively, found in our experimental data. Here, we reconciled these theoretical findings by reconstructing the thalamocortical projections across the visual hierarchy. This was achieved by connecting with different strengths the output of excitatory neurons of the LP to the excitatory or inhibitory neurons of the simulated visual cortex. The model of the present work also proposes two possible scenarios of excitatory-inhibitory connectivity between the LP and the visual cortex that simultaneously change the response gain across the visual hierarchy. The fact that the pulvinar produces opposite effects in low and high areas shows that this thalamic nucleus has an active role in the transmission of visual activity along the visual cortex (Shipp 2003). These hypothetical outlines should be verified by future anatomical and physiological discoveries of the transthalamic pathway. Together, these findings suggest that the role of the transthalamic pathway is to functionally shortcut the visual contrast information from lower to higher levels of the cortical hierarchy. The LP may act as an active blackboard informing the visual cortex (Mumford 1991). While this shortcut may speed up the transmission of information across the hierarchy, it would also maintain “up-to-date” the visual cortex with new inputs. Thus, the short circuit by the LP would allow cortical areas to be informed of any relevant changes of the external visual world (Casanova 2004).

It is well known that the pulvinar participates in modulatory visual processes such as attention and visual salience (Petersen et al. 1987; Desimone et al. 1990; Robinson and Petersen 1992; Saalmann and Kastner 2009, 2011; Snow et al. 2009; Saalmann et al. 2012). In the primate area V4, a homolog of area 21a in cats (Payne 1993), the neuronal responses are extensively modulated by attention (Saalmann et al. 2012; Zhou et al. 2016). Previous studies reported changes on the CRF of V4 neurons when animals were engaged in attention-demanding tasks (Reynolds and Desimone 1999; Reynolds et al. 2000; Williford and Maunsell 2006; Hudson et al. 2009). Interestingly, one study (Williford and Maunsell 2006) demonstrated that the attentional modulation of the contrast response of neurons from V4 was predominantly characterized by changes on the response gain. Recent evidence indicated that the pulvinar mediates the attentional effects in area V4 (Zhou et al. 2016). Thus, one may hypothesize that the pulvinar plays an essential role in the attentional modulation of the contrast response in area V4. In our study, experiments were carried out in anesthetized cats and one should be cautious in discussing the data in the context of attentional processes. However, we believe that the neuronal circuits and mechanisms underlying the changes observed here may be those involved in awake animals. Zhou et al. (2016) observed that the pulvinar inactivation affected the neuronal responses in area V4 regardless of the attentional effects suggesting that the pulvinar is actively implicated in the basic processing of visual information in this cortical area. Indeed, this was corroborated by our findings supporting the notion that the pulvinar is actively implicated in the modulation of the visual processing in extrastriate areas of the ventral stream.

The pulvino-cortical connections are part of distinct transthalamic networks involved in different sensory modalities (Abramson and Chalupa 1985; Eördegh et al. 2005; Llano and Sherman 2008; Theyel et al. 2010; Sherman and Guillery 2011). Most studies focused on the anatomical and functional properties of corticothalamic connections involving visual (Casanova et al. 1997), somatosensory (Reichova and Sherman 2004) and auditory (Llano and Sherman 2008) areas. On the other hand, less is known about the nature of reciprocal thalamocortical projections involving higher-order thalamic nuclei such as the pulvinar. For instance, in brain slices of mice, the activation/deactivation of transthalamic pathways involving the posterior medial nucleus (POm) yielded a significant increase and decrease in the neuronal activity of an extrastriate area of the somatosensory cortex (Theyel et al. 2010) suggesting that these projections were a driver in nature. Our findings are at odds with this study since the main impact of the LP inactivation was modulatory. However, it is difficult to reconcile our findings with those from Theyel et al. (2010) since experiments were undertaken on different species (cat vs. mouse), experimental setting (in vivo vs. in vitro), and thalamic nuclei (LP vs. POm).

The present study demonstrates that the pulvinar influences cortical functions across the ventral stream mainly by modulating neuronal activity. Furthermore, our findings provide evidence on the possible mechanisms underlying the transthalamic flow of information and its role in cortical contrast processing. The pulvinar is extensively connected with several cortical areas that perform high level sensory and cognitive processes. Thus, knowing the nature of cortico-pulvino-cortical connections is essential for understanding the mechanisms subtending visual perception and its pathological states.

Funding

Canadian Institute for Health Research (CIHR) (grant PJT-148959 to C.C.), EOUM-FESP scholarships (to B.O.F.S.), and the Chilean fellowship BecasChile and CONICYT (to N.C.).

Notes

This article is dedicated to Umit Keysan (1992–2019), a wonderful friend and student. We thank Geneviève Cyr for her technical help and Alessandro Barry for comments on the theoretical model.

References

Abbott LF, Chance FS. 2005. Drivers and modulators from push-pull and balanced synaptic input. *Prog Brain Res*. 149:147–155.

Abramson BP, Chalupa LM. 1985. The laminar distribution of cortical connections with the tecto- and cortico-recipient zones in the cat's lateral posterior nucleus. *Neuroscience*. 15: 81–95.

Anderson JS, Carandini M, Ferster D. 2000. Orientation tuning of input conductance, excitation, and inhibition in cat primary visual cortex. *J Neurophysiol*. 84:909–926.

Arcaro MJ, Pinsk MA, Kastner S. 2015. The anatomical and functional Organization of the Human Visual Pulvinar. *J Neurosci*. 35:9848–9871.

Avidan G, Harel M, Hendler T, Ben-Bashat D, Zohary E, Malach R. 2002. Contrast sensitivity in human visual areas and its relationship to object recognition. *J Neurophysiol*. 87:3102–3116.

Barron DS, Eickhoff SB, Clos M, Fox PT. 2015. Human pulvinar functional organization and connectivity. *Hum Brain Mapp*. 36:2417–2431, 7, DOI: 10.1002/hbm.22781.

Benarroch E. 2015. Pulvinar: associative role in cortical function and clinical correlations. *Neurology*. 84:738–747.

Bender D. 1983. Visual activation of neurons in the primate pulvinar depends on cortex but not colliculus. *Brain Res*. 279:258–261.

Benevento LA, Rezak M. 1976. The cortical projections of the inferior pulvinar and adjacent lateral pulvinar in the rhesus monkey (macaca mulatta): an autoradiographic study. *Brain Res*. 108:1–24.

Berson DM, Graybiel AM. 1983. Organization of the striate-recipient zone of the cat's lateralis posterior-pulvinar complex and its relations with the geniculostriate system. *Neuroscience*. 9:337–372.

Brette R, Gerstner W. 2005. Adaptive exponential integrate-and-fire model as an effective description of neuronal activity. *J Neurophysiol*. 94:3637–3642.

Burkhardt DA. 2011. Contrast processing by ON and OFF bipolar cells. *Vis Neurosci*. 28:69–75.

Byne W, Hazlett EA, Buchsbaum MS, Kemether E. 2009. The thalamus and schizophrenia: current status of research. *Acta Neuropathol*. 117:347–368.

Casanova C. 1993. Response properties of neurons in area-17 projecting to the striate-recipient zone of the cats lateralis posterior-pulvinar complex - comparison with cortico-tectal cells. *Exp Brain Res*. 96:247–259.

Casanova C. 2004. The visual functions of the pulvinar. In: *The visual neurosciences*. In Cambridge, MA: MIT Press, pp. 592–608.

Casanova C, Savard T. 1996. Motion sensitivity and stimulus interactions in the striate-recipient zone of the cat's lateral posterior-pulvinar complex. *Prog Brain Res*. 112:277–287.

Casanova C, Savard T, Darveau S. 1997. Contribution of area 17 to cell responses in the striate-recipient zone of the cat's lateral posterior-pulvinar complex. *Eur J Neurosci*. 9:1026–1036.

Cavanaugh J, Bair W, Movshon J. 2002. Nature and interaction of signals from the receptive field center and surround in macaque V1 neurons. *J Neurophysiol*. 88:2530–2546.

Chalfin BP, Cheung DT, Muniz JAPC, de Lima Silveira LC, Finlay BL. 2007. Scaling of neuron number and volume of the pulvinar complex in new world primates: comparisons with humans, other primates, and mammals. *J Comp Neurol*. 504:265–274.

Chalupa LM, Abramson BP. 1989. Visual receptive fields in the striate-recipient zone of the lateral posterior-pulvinar complex. *J Neurosci*. 9:347–357.

Chalupa LM, Williams RW, Hughes MJ. 1983. Visual response properties in the tectorecipient zone of the cat's lateral posterior-pulvinar complex: a comparison with the superior colliculus. *J Neurosci*. 3:2587–2596.

Chance FS, Abbott LF, Reyes AD. 2002. Gain modulation from background synaptic input. *Neuron*. 35:773–782.

Cortes N, van Vreeswijk C. 2015. Pulvinar thalamic nucleus allows for asynchronous spike propagation through the cortex. *Front Comput Neurosci*. 9, DOI: 10.3389/fncom.2015.00060.

Cortes NH, Van Vreeswijk C. 2012. The role of pulvinar in the transmission of information in the visual hierarchy. *Front Comput Neurosci*. 6:29.

Crick F, Koch C. 1998. Constraints on cortical and thalamic projections: the no-strong-loops hypothesis. *Nature*. 391: 245–250.

Cutrone EK, Heeger DJ, Carrasco M. 2014. Attention enhances contrast appearance via increased input baseline of neural responses. *J Vis*. 14:16.

Desimone R, Wessinger M, Thomas L, Schneider W. 1990. Attentional control of visual perception: cortical and subcortical mechanisms. *Cold Spring Harb Symp Quant Biol*. 55:963–971.

Dreher B, Djavadian RL, Turlejski KJ, Wang C. 1996. Areas PMLS and 21a of cat visual cortex are not only functionally but also hodologically distinct. *Prog Brain Res*. 112:251–276.

Dreher B, Michalski A, Ho RH, Lee CW, Burke W. 1993. Processing of form and motion in area 21a of cat visual cortex. *Vis Neurosci*. 10:93–115.

Enroth-Cugell C, Robson JG. 1966. The contrast sensitivity of retinal ganglion cells of the cat. *J Physiol*. 187:517–552.

Eördegh G, Nagy A, Berényi A, Benedek G. 2005. Processing of spatial visual information along the pathway between the suprageniculate nucleus and the anterior ectosylvian cortex. *Brain Res Bull*. 67:281–289.

Felleman DJ, Van Essen DC. 1991. Distributed hierarchical processing in the primate cerebral cortex. *Cereb Cortex*. 1:1–47.

Gabbiani F, Midtgaard J, Knopfel T. 1994. Synaptic integration in a model of cerebellar granule cells. *J Neurophysiol*. 72: 999–1009.

Gabbott PL, Somogyi P. 1986. Quantitative distribution of GABA-immunoreactive neurons in the visual cortex (area 17) of the cat. *Exp Brain Res*. 61:323–331.

Goris RLT, Movshon JA, Simoncelli EP. 2014. Partitioning neuronal variability. *Nat Neurosci*. 17:858–865.

Graybiel AM, Berson DM. 1980. Histochemical identification and afferent connections of subdivisions in the lateralis posterior-pulvinar complex and related thalamic nuclei in the cat. *Neuroscience*. 5:1175–1238.

Haider B, Duque A, Hasenstaub AR, McCormick DA. 2006. Neocortical network activity in vivo is generated through a dynamic balance of excitation and inhibition. *J Neurosci*. 26: 4535–4545.

Haider B, Krause MR, Duque A, Yu Y, Touryan J, Mazer JA, McCormick DA. 2010. Synaptic and network mechanisms of sparse and reliable visual cortical activity during nonclassical receptive field stimulation. *Neuron*. 65:107–121.

Hudson AE, Schiff ND, Victor JD, Purpura KP. 2009. Attentional modulation of adaptation in V4. *Eur J Neurosci*. 30: 151–171.

Huppé-Gourgues F, Bickford ME, Boire D, Ptito M, Casanova C. 2006. Distribution, morphology, and synaptic targets of corticothalamic terminals in the cat lateral posterior-pulvinar complex that originate from the posteromedial lateral suprasylvian cortex. *J Comp Neurol*. 497:847–863.

Hutchins B, Updyke BV. 1989. Retinotopic organization within the lateral posterior complex of the cat. *J Comp Neurol*. 285:350–398.

Ji X, Zingg B, Mesik L, Xiao Z, Zhang LI, Tao HW. 2016. Thalamocortical innervation pattern in mouse auditory and visual cortex: laminar and cell-type specificity. *Cereb Cortex*. 26:2612–2625.

Jones EG. 2001. The thalamic matrix and thalamocortical synchrony. *Trends Neurosci*. 24:595–601.

Kandel E, Schwartz J. 2013. *Principles of neural science*. 5th ed. New York, NY: McGraw Hill Professional.

Kumar A, Rotter S, Aertsen A. 2010. Spiking activity propagation in neuronal networks: reconciling different perspectives on neural coding. *Nat Rev Neurosci*. 11:615–627.

Lai J, Legault M-A, Thomas S, Casanova C. 2015. Simultaneous electrophysiological recording and micro-injections of inhibitory agents in the rodent brain. *J Vis Exp*. DOI: 10.3791/52271

Lee CC, Sherman SM. 2008. Synaptic properties of thalamic and Intracortical inputs to layer 4 of the first- and higher-order cortical areas in the auditory and somatosensory systems. *J Neurophysiol*. 100:317–326.

Leh SE, Chakravarty MM, Ptito A. 2008. The connectivity of the human pulvinar: a diffusion tensor imaging tractography study. *Int J Biomed Imaging*. 2008:789539.

Ling S, Carrasco M. 2006. Sustained and transient covert attention enhance the signal via different contrast response functions. *Vision Res*. 46:1210–1220.

Litvak V, Sompolinsky H, Segev I, Abeles M. 2003. On the transmission of rate code in long feedforward networks with excitatory-inhibitory balance. *J Neurosci*. 23:3006–3015.

Llano DA, Sherman SM. 2008. Evidence for nonreciprocal organization of the mouse auditory thalamocortical-corticothalamic projection systems. *J Comp Neurol*. 507: 1209–1227.

Lund JS, Lund RD, Hendrickson AE, Bunt AH, Fuchs AF. 1975. The origin of efferent pathways from the primary visual cortex, area 17, of the macaque monkey as shown by retrograde transport of horseradish peroxidase. *J Comp Neurol*. 164:287–303.

Merabet L, Desautels A, Minville K, Casanova C. 1998. Motion integration in a thalamic visual nucleus. *Nature*. 396:265–268.

Miller JW, Buschmann MBT, Benevento LA. 1980. Extrageniculate thalamic projections to the primary visual cortex. *Brain Res*. 189:221–227.

Minville K, Casanova C. 1998. Spatial frequency processing in posteromedial lateral suprasylvian cortex does not depend on the projections from the striate-recipient zone of the cat's lateral posterior-pulvinar complex. *Neuroscience*. 84:699–711.

Molotchnikoff S, Shumikhina S. 1996. The lateral posterior-pulvinar complex modulation of stimulus-dependent oscillations in the cat visual cortex. *Vision Res*. 36:2037–2046.

Morley JW, Vickery RM. 1997. Spatial and temporal frequency selectivity of cells in area 21a of the cat. *J Physiol*. 501: 405–413.

Movshon JA, Thompson ID, Tolhurst DJ. 1978. Spatial and temporal contrast sensitivity of neurones in areas 17 and 18 of the cat's visual cortex. *J Physiol*. 283:101–120.

Mumford D. 1991. On the computational architecture of the neocortex I. *The role of the thalamocortical loop*. *Biol Cybern*. 65:135–145.

Naka KI, Rushton WAH. 1966. S-potentials from colour units in the retina of fish (Cyprinidae). *J Physiol*. 185:536–555.

Ogren MP, Hendrickson AE. 1977. The distribution of pulvinar terminals in visual areas 17 and 18 of the monkey. *Brain Res*. 137:343–350.

Panagiotaropoulos TI, Kapoor V, Logothetis NK. 2014. Subjective visual perception: from local processing to emergent phenomena of brain activity. *Philos Trans R Soc B Biol Sci*. 369:20130534.

Payne BR. 1993. Evidence for visual cortical area homologs in cat and macaque monkey. *Cereb Cortex*. 3:1–25.

Petersen SE, Robinson DL, Morris JD. 1987. Contributions of the pulvinar to visual spatial attention. *Neuropsychologia*. 25:97–105.

Purushothaman G, Marion R, Li K, Casagrande VA. 2012. Gating and control of primary visual cortex by pulvinar. *Nat Neurosci*. 15:905–912.

Raczkowski D, Rosenquist AC. 1983. Connections of the multiple visual cortical areas with the lateral posterior-pulvinar complex and adjacent thalamic nuclei in the cat. *J Neurosci*. 3:1912–1942.

Reichova I, Sherman S. 2004. Somatosensory corticothalamic projections: distinguishing drivers from modulators. *J Neurophysiol*. 92:2185–2197.

Reynolds JH, Desimone R. 1999. The role of neural mechanisms of attention in solving the binding problem. *Neuron*. 24:19–29.

Reynolds JH, Pasternak T, Desimone R. 2000. Attention increases sensitivity of V4 neurons. *Neuron*. 26:703–714.

Rezak M, Benevento LA. 1979. A comparison of the organization of the projections of the dorsal lateral geniculate nucleus, the inferior pulvinar and adjacent lateral pulvinar to primary visual cortex (area 17) in the macaque monkey. *Brain Res*. 167:19–40.

Rinvik E, Ottersen OP, Storm-Mathisen J. 1987. Gamma-aminobutyrate-like immunoreactivity in the thalamus of the cat. *Neuroscience*. 21:781–805.

Robinson DL, Petersen SE. 1992. The pulvinar and visual salience. *Trends Neurosci*. 15:127–132.

Rossant C, Kadir SN, Goodman DFM, Schulman J, Hunter MLD, Saleem AB, Grosmark A, Belluscio M, Denfield GH, Ecker AS *et al*. 2016. Spike sorting for large, dense electrode arrays. *Nat Neurosci*. 19:634–641.

Roth MM, Dahmen JC, Muir DR, Imhof F, Martini FJ, Hofer SB. 2016. Thalamic nuclei convey diverse contextual information to layer 1 of visual cortex. *Nat Neurosci*. 19:299–307, 2, DOI: 10.1038/nn.4197.

Saalmann YB, Kastner S. 2009. Gain control in the visual thalamus during perception and cognition. *Curr Opin Neurobiol*. 19:408–414.

Saalmann YB, Kastner S. 2011. Cognitive and perceptual functions of the visual thalamus. *Neuron*. 71:209–223.

Saalmann YB, Pinsk MA, Wang L, Li X, Kastner S. 2012. The Pulvinar regulates information transmission between cortical areas based on attention demands. *Science*. 337:753–756.

Sakata S, Harris KD. 2009. Laminar structure of spontaneous and sensory-evoked population activity in auditory cortex. *Neuron*. 64:404–418.

Sani I, Santandrea E, Golzar A, Morrone MC, Chelazzi L. 2013. Selective tuning for contrast in macaque area V4. *J Neurosci*. 33:18583–18596.

Scannell J, Blakemore C, Young M. 1995. Analysis of connectivity in the cat cerebral cortex. *J Neurosci*. 15:1463–1483.

Sherman SM, Guillery RW. 1996. Functional organization of thalamocortical relays. *J Neurophysiol*. 76:1367–1395.

Sherman SM, Guillery RW. 1998. On the actions that one nerve cell can have on another: Distinguishing "drivers" from "modulators." *Proc Natl Acad Sci*. 95:7121–7126.

Sherman SM, Guillery RW. 2011. Distinct functions for direct and transthalamic corticocortical connections. *J Neurophysiol*. 106:1068–1077.

Sherman SM, Guillery RW. 2013. *Functional connections of cortical areas: a new view from the thalamus*. Cambridge, MA: MIT Press.

Shipp S. 2003. The functional logic of cortico-pulvinar connections. *Philos Trans R Soc B Biol Sci*. 358:1605–1624.

Siegle JH, López AC, Patel YA, Abramov K, Ohayon S, Voigts J. 2017. Open Ephys: an open-source, plugin-based platform for multichannel electrophysiology. *J Neural Eng*. 14: 045003.

Sirota A, Montgomery S, Fujisawa S, Isomura Y, Zugaro M, Buzsáki G. 2008. Entrainment of neocortical neurons and gamma oscillations by the hippocampal theta rhythm. *Neuron*. 60:683–697.

Skottun BC, De Valois RL, Grosof DH, Movshon JA, Albrecht DG, Bonds AB. 1991. Classifying simple and complex cells on the basis of response modulation. *Vision Res*. 31:1078–1086.

Snow JC, Allen HA, Rafal RD, Humphreys GW. 2009. Impaired attentional selection following lesions to human pulvinar: evidence for homology between human and monkey. *Proc Natl Acad Sci*. 106:4054–4059.

Soares J, Diogo A, Fiorani M, Souza A, Gattass R. 2004. Effects of inactivation of the lateral pulvinar on response properties of second visual area cells in Cebus monkeys. *Clin Exp Pharmacol Physiol*. 31:580–590.

Soma S, Shimegi S, Suematsu N, Tamura H, Sato H. 2013. Modulation-specific and laminar-dependent effects of acetylcholine on visual responses in the rat primary visual cortex. *PLoS ONE*. 8, DOI: 10.1371/journal.pone.0068430.

de Souza BOF, Casanova C. 2019. Stronger responses to darks along the ventral pathway of the cat visual cortex. *Eur J Neurosci*. 0:1–13.

Stimberg M, Goodman DFM, Benichoux V, Brette R. 2014. Equation-oriented specification of neural models for simulations. *Front Neuroinf*. 8:6.

Symonds LL, Rosenquist AC, Edwards SB, Palmer LA. 1981. Projections of the pulvinar-lateral posterior complex to visual cortical areas in the cat. *Neuroscience*. 6:1995–2020.

Tardif E, Bergeron A, Lepore F, Guillemot J-P. 1996. Spatial and temporal frequency tuning and contrast sensitivity of single neurons in area 21a of the cat. *Brain Res*. 716:219–223, 1-2, DOI: 10.1016/0006-8993(96)00031-5.

Theyel BB, Llano DA, Sherman M. 2010. The corticothalamocortical circuit drives higher-order cortex in the mouse. *Nat Neurosci*. 13:84–88.

Trojanowski JQ, Jacobson S. 1977. The morphology and laminar distribution of cortico-pulvinar neurons in the rhesus monkey. *Exp Brain Res*. 28:51–62.

Van Der Gucht E, Vandesande F, Arckens L. 2001. Neurofilament protein: a selective marker for the architectonic parcellation of the visual cortex in adult cat brain. *J Comp Neurol*. 441:345–368.

Viaene AN, Petrof I, Sherman SM. 2011. Synaptic properties of thalamic input to the subgranular layers of primary somatosensory and auditory cortices in the mouse. *J Neurosci Off J Soc Neurosci*. 31:12738–12747.

Vickery RM, Morley JW. 1999. Binocular phase interactions in area 21a of the cat. *J Physiol*. 514:541–549.

Villeneuve MY, Casanova C. 2003. On the use of isoflurane versus halothane in the study of visual response properties of single cells in the primary visual cortex. *J Neurosci Methods*. 129:19–31.

Villeneuve MY, Vanni MP, Casanova C. 2009. Modular organization in area 21a of the cat revealed by optical imaging: comparison with the primary visual cortex. *Neuroscience*. 164:1320–1333.

Vogels TP, Abbott LF. 2009. Gating multiple signals through detailed balance of excitation and inhibition in spiking networks. *Nat Neurosci*. 12:483–491.

van Vreeswijk C, Sompolinsky H. 1996. Chaos in neuronal networks with balanced excitatory and inhibitory activity. *Science*. 274:1724–1726.

Ward R, Danziger S, Owen V, Rafal R. 2002. Deficits in spatial coding and feature binding following damage to spatiotopic maps in the human pulvinar. *Nat Neurosci*. 5: 99–100.

Williford T, Maunsell JHR. 2006. Effects of spatial attention on contrast response functions in macaque area V4. *J Neurophysiol*. 96:40–54.

Wilson FA, O'Scalaidhe SP, Goldman-Rakic PS. 1994. Functional synergism between putative gamma-aminobutyrate-containing neurons and pyramidal neurons in prefrontal cortex. *Proc Natl Acad Sci*. 91:4009–4013.

Wimborne BM, Henry GH. 1992. Response characteristics of the cells of cortical area 21a of the cat with special reference to orientation specificity. *J Physiol*. 449:457–478.

Zhang J, Zhang X, Hu X, Wu W, Yang Y. 2017. Organization of spatial frequency in cat striate cortex. *Neuroscience*. 362: 95–103.

Zhou H, Schafer RJ, Desimone R. 2016. Pulvinar-cortex interactions in vision and attention. *Neuron*. 89:209–220.